Hindawi
Advances in Condensed Matter Physics
Volume 2018, Article ID 3898479, 29 pages
https://doi.org/10.1155/2018/3898479

Review Article

Carbon-Based Materials for Thermoelectrics

Pranay Chakraborty, Tengfei Ma, Amir Hassan Zahiri, Lei Cao, and Yan Wang

Department of Mechanical Engineering, University of Nevada, Reno, NV 89557, USA

Correspondence should be addressed to Yan Wang; yanwang@unr.edu

Received 12 February 2018; Accepted 13 May 2018; Published 4 July 2018

Academic Editor: Markus R. Wagner

This article reviews the recent progress towards achieving carbon-based thermoelectric materials. A wide range of experimental and computational studies on carbon allotropes and composites is covered in this review paper. Specifically, we discuss the strategies for engineering graphene, graphene nanoribbon, graphene nanomesh, graphene nanowiggle, carbon nanotube (CNT), fullerene, graphyne, and carbon quantum dot for better thermoelectric performance. Moreover, we discuss the most recent advances in CNT/graphene-polymer composites and the related challenges and solutions. We also highlight the important charge and heat transfer mechanisms in carbon-based materials and state-of-the-art strategies for enhancing thermoelectric performance. Finally, we provide an outlook towards the future of carbon-based thermoelectrics.

1. Introduction

Thermoelectric (TE) material can convert heat into electricity directly. This power generation capability stems from the Seebeck effect, which was discovered originally by Alessandro Volta in 1787 and rediscovered independently by Thomas Johann Seebeck in 1821 [1]. According to the energy flow chart published by the Lawrence Livermore National Laboratory [2], about two-thirds of energy was wasted as heat in the United States in 2016. Obviously, it would lead to huge economic benefits to the society if highly efficient TE materials can be created and utilized in a wide range of applications. In addition to the Seebeck effect, TE effect can also be manifested as the Peltier effect and the Thomson effect. In the former, electric current drives heat flow from one end to the other end of the TE module, while in the latter, the entire TE module can be cooled by a dc current when a temperature gradient exists. Both the Seebeck effect and the Thomson effect can be used for solid-state cooling technology. This is advantageous over conventional refrigerators and air conditioners composed of bulky compressors and condensers, which produce considerable amount of noise and are prone to mechanical failure owing to the cyclically moving components.

The efficiency of TE materials can be measured by the dimensionless figure of merit (ZT), which is defined as

$$ZT = \frac{\sigma S^2 T}{\kappa_e + \kappa_L}, \tag{1}$$

in which σ is the electrical conductivity, S is the Seebeck coefficient (also commonly referred to as thermopower or thermoelectric power), T is the absolute temperature, κ_e is the electronic thermal conductivity, and κ_L is the lattice thermal conductivity. In addition to efficiency, we can also quantify the effectiveness of the TE materials by power factor, which is defined as

$$\text{Power factor} = \sigma S^2. \tag{2}$$

It has been estimated that TE materials must have a ZT higher than 3 to compete with traditional energy conversion technologies and coolers in terms of power efficiency. Nonetheless, the highest ZT obtained so far is only ~2.6 (at 923 K) [3] while the highest room-temperature ZT is even lower. Therefore, developing strategies for increasing the ZT remains an active and important research subject. Noting that σ and κ_e are typically related via the Wiedemann-Franz law,

$$\kappa_e = LT\sigma, \tag{3}$$

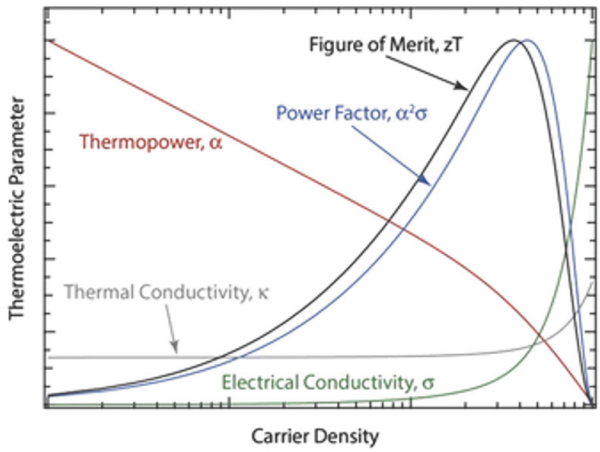

Figure 1: Schematic showing the coupled dependence of the various TE properties on carrier density. The shape of each individual curve was extracted from actual data on single-walled carbon nanotube networks. Figure reproduced with permission [5].

in which L is the Lorenz number, (1) can be transformed into

$$ZT = \frac{S^2}{L + \kappa_L/\sigma T}. \quad (4)$$

Evidently, based on (4), minimizing the ratio between κ_L and σ can lead to optimized ZT of TE materials. This is the famous "phonon-glass, electron-crystal" (PGEC) paradigm [4], which asserts that good TE materials should facilitate charge transport like a semiconductor crystal while blocking phononic heat transfer like a glass. In addition to the PGEC paradigm, it is also attractive to increase the Seebeck coefficient S of materials through various mechanisms, for example, electron energy filtering or band structure engineering. Indeed, it is usually challenging to significantly enhance the ZT of materials in this manner, because S and σ are usually strongly correlated with each other. Similarly, strategies for reducing $\kappa_L$often come with the sacrifice of σ. The interdependence between the TE properties of carbon nanotube networks [5] is qualitatively shown in Figure 1 as an example.

There are a large variety of bulk TE materials that are under investigation, including singe phase and alloys of lead chalcogenides (PbX, X = S, Se, or Te) [6–11], binary skutterudites (MX_3, M = Co, Rh or Ir; X = P, As, or Sb) [12–14], clathrates [15], copper chalcogenides ($Cu_{2-x}X$, X = S, Se, or Te) [16], oxides (e.g., $NaxCoO_2$, ZnO, and Ruddlesden-Popper homologous series) [17–20], half-Heusler compounds [21, 22], Bi_2Te_3/Sb_2Te_3 [23, 24], SiGe [25], and SnSe [3]. All these bulk TE materials are characterized by a low lattice thermal conductivity, partly or primarily owing to the strong lattice anharmonicity, small phonon group velocity, or extensive phonon scattering by various lattice defects. The two pioneering papers by Hicks and Dresselhaus that were published in 1993 revealed that 1D and 2D structures could carry much higher figure-of-merit ZT than conventional 3D forms of the material [26, 27], which triggered the extensive exploration of nanostructured low-dimensional TE materials [28]. In many cases, nanostructuring of TE materials can break the ZT limit of bulk materials by reducing the lattice thermal conductivity or increasing the Seebeck coefficient. For example, quantum dots [29], nanowires [30, 31], and layered structures [32–34] are some of the structures that have been found experimentally or predicted theoretically to possess much lower κ_L or higher ZT than their bulk counterparts. The underlying mechanism for the greatly reduced κ_L of these nanostructures lies in one or several of the following factors: classical size effect, quantum size effect, and phonon localization, which can significantly hinder phonon transport [35]. However, the high manufacturing cost, scarcity, toxicity, instability, and unsatisfactory ZT of some or most of the TE materials discussed above prevent them from being an immediate solution to the current energy crisis. Moreover, TE components are subject to considerable thermoelastic stress, mechanical vibration, thermal transients, and even thermal shock during service, necessitating the requirement of strong and tough TE materials. Nonetheless, most of the TE materials mentioned above will crack or fracture during cyclic thermal loading due to the brittleness.

Carbon-based materials, in contrast to the conventional TE materials mentioned above, typically exhibit high flexibility, fracture toughness, high strength, and high-temperature stability. Carbon has a variety of allotropes owing to its capability of hybridization in sp, sp^2, and sp^3 bonds, which renders it able to form 0D (e.g., fullerenes), 1D (e.g., carbon nanotube), 2D (e.g., graphene), and 3D (e.g., diamond) structures and thus one of the most versatile elements in the periodic table. Moreover, carbon is one of the most abundant elements on earth (15th among all elements) and most of its allotropes are nontoxic and lightweight. Even though diamond and graphene are well known to have ultrahigh κ_L (Figure 2), which excludes them as TE materials in their pristine form, nanoengineering can reduce the κ_L of certain carbon allotropes significantly [36, 37]. Therefore, it is of great interest and potential to investigate carbon-based nanomaterials for TE applications. Here in this article we will focus on recently developed or proposed carbon-based nanomaterials as TE materials. We will discuss their advantages and disadvantages over the commonly used materials and possible ways of improving the ZT of these carbon-based TE materials. We will limit the scope of this work to materials just composed of carbon atoms or with minor decorations with other elements, because there also exist a large variety of polymer-based TE materials. We refer interested readers to [38–40] for organic TE materials, which are also under extensive study owing to their low-cost, structural flexibility, and potential for printable and scalable manufacturing.

This review paper is organized as follows. In Section 2, basics of thermoelectric materials, such as thermoelectricity, lattice thermal transport, and mechanical properties, will be discussed. In Section 3, we will provide an overview of TE materials primarily based on single-material carbon allotropes. In Section 4, we will review TE materials combining one or more carbon allotropes with other materials like polymer into a composite. Finally, we will provide an outlook towards future research on carbon-based TE materials and conclude this review.

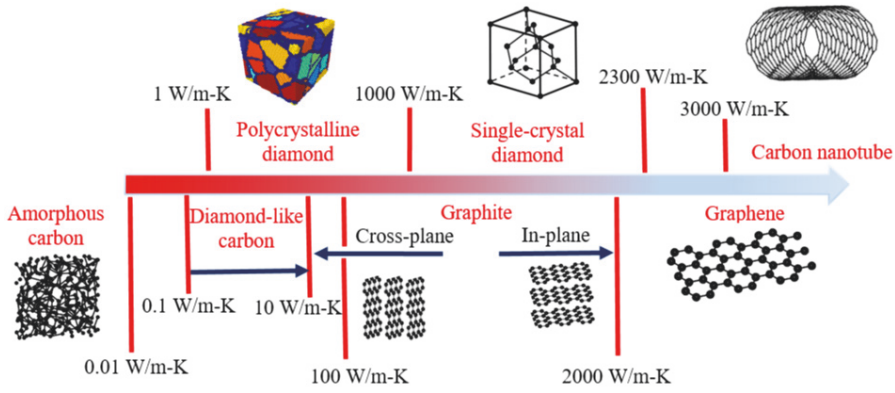

Figure 2: Illustration of the wide distribution of the thermal conductivity of carbon-based materials.

2. Basics of Thermoelectric Materials

2.1. Thermoelectricity. The origin of thermoelectricity can be understood in several ways. The Boltzmann transport equations (BTE), being a popular and effective way for treating electron transport, are commonly adopted by textbooks and review papers on thermoelectricity. The general forms of the equations used for calculating TE properties from first principles are [41–43]

$$\Sigma(E) = \sum_{n,\vec{k}} v^2\left(n,\vec{k}\right)\tau\left(n,\vec{k}\right)\delta\left[E - E\left(n,\vec{k}\right)\right], \quad (5)$$

$$\sigma = -e^2\int \Sigma(E)\frac{\partial f_{FD}}{\partial E}dE, \quad (6)$$

$$S = -\frac{e}{T\sigma}\int (E-\mu)\,\Sigma(E)\frac{\partial f_{FD}}{\partial E}dE, \quad (7)$$

and

$$L = -\frac{1}{T^2\sigma}\int (E-\mu)^2\,\Sigma(E)\frac{\partial f_{FD}}{\partial E}dE. \quad (8)$$

In (5)–(8), $\Sigma(E)$ is the energy-dependent transport distribution function, $v(n,\vec{k})$ and $\tau(n,\vec{k})$ are the velocity and relaxation time of an electron (or hole) in the n'th band and with a wavevector of $\vec{k}$, δ is the delta function, E is electron energy, μ is chemical potential, σ is the electrical conductivity, e is the charge of electron, S is the Seebeck coefficient, T is the absolute temperature, and L is the Lorentz constant already used in (3) and (4). In the above equations, f_{FD} is the Fermi-Dirac distribution function, which is

$$f_{FD}(E,T) = \frac{1}{e^{(E-\mu)/k_BT}+1}, \quad (9)$$

where k_B is the Boltzmann constant. According to (8), the value of L is dependent on several factors, such as the shape of band structure, chemical potential, and temperature. In fact, it can be shown that L converges to a constant value (Sommerfeld limit) of

$$L = \frac{\pi^2}{3}\left(\frac{k_B}{e}\right)^2 = 2.44\times10^{-8}\,\mathrm{W\Omega/K^2}, \quad (10)$$

in the degenerate limit (metals and heavily doped semiconductors). In the nondegenerate limit, however, L depends on the type of scatterings and shape of band structures. For example, it converges to $1.5\times10^{-8}\,\mathrm{W\Omega/K^2}$ for nondegenerate semiconductors with a parabolic band and acoustic phonon scattering, while it changes with various parameters (chemical potential, band structure, etc.) for semiconductors between the degenerate and nondegenerate limits [44].

Despite the practicability of BTE for evaluating TE properties of materials from first principles, the basic idea of thermoelectricity is usually buried by the complexity of those equations. Here, we choose to use a bottom-up approach, which is also known as the Landauer-Datta-Lundstrom model [45], to demonstrate the origin of thermoelectricity and illustrate the idea of "best thermoelectric materials" to the more general audience.

The Landauer-Datta-Lundstrom model starts from the elastic resistor concept. Figure 3(a) shows an electronic device composed of an elastic channel (no carrier scattering) sandwiched by two ideal contacts. The channel and contacts are made of exactly the same materials and the only difference between them is either the temperature or the chemical potential. Besides, we assume that the channel has a typical 3D electron density of states $D(E)$ as shown in Figure 3(a), while the electron statistics in the two contacts follow the Fermi-Dirac distribution $f_{FD}(E,T)$ described by (9). If the two contacts have different chemical potential μ as a result of an external electrical voltage $\Delta V = \mu_2 - \mu_1 < 0$, there will be a shift along the E axis between the two f_{FD}'s. Evidently, the difference, $f_{FD,1} - f_{FD,2}$, is positive and is significant for $\mu_2 < E < \mu_1$. In other words, the value of f_{FD} or the number density of electron $D(E)f_{FD}$ at the left contact is always higher than that at the right contact at any energy level E, especially for $\mu_2 < E < \mu_1$. As a result, the left contact will keep feeding electrons to the right through the channel and vice versa for

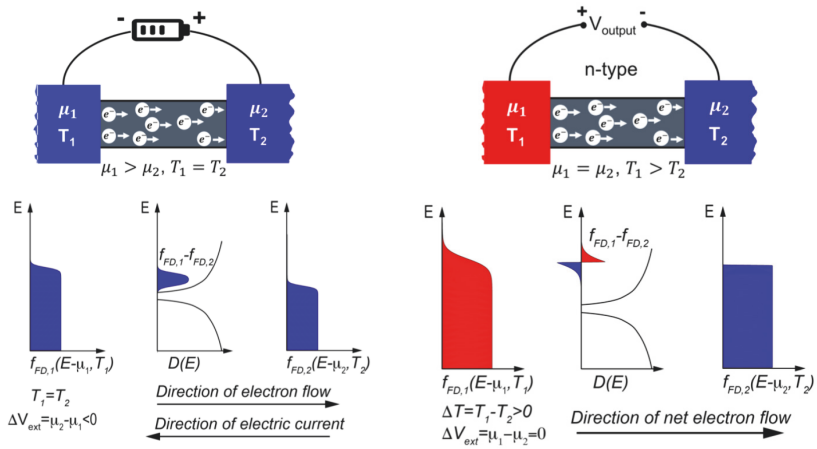

(a) Conductor under external voltage V_{ext} (b) n-type TE generator under temperature bias

FIGURE 3: Origin of electricity under an external electrical bias (voltage) and thermoelectricity under a temperature bias. (a) A typical elastic conductor in the Landauer-Datta-Lundstrom model, in which a voltage V_{ext} is exerted by an external power source, e.g., battery. An electric current is resulted from the external electric bias, owing to the mismatch between the Fermi-Dirac distributions of the two contacts. (b) Schematic of an n-type thermoelectric generator consisting of two contacts maintained at different temperatures. The temperature bias causes a difference in the shape of the Fermi-Dirac distributions at the two contacts, thus leading to thermoelectricity.

the right contact. An electron current I_e thus results from such nonequilibrium. Mathematically, the above analysis of I_e can be quantified as

$$I_e = \int G(E)\left[f_{FD,1}(\mu_1, T_1) - f_{FD,2}(\mu_2, T_2)\right] dE, \quad (11)$$

in which $G(E)$ is the conductance at energy level E and is proportional to the electron density of states $D(E)$, as discussed in [45].

The case for thermoelectricity can be analyzed in a similar way. As shown in Figure 3(b), $f_{FD,1} - f_{FD,2}$ is nonzero when there is a temperature difference between the two contacts, even though their chemical potential is equal (no external electrical bias). Unlike the symmetric profile in Figure 3(a), $f_{FD,1} - f_{FD,2}$ is antisymmetric, which means that some electric current (red region of $f_{FD,1} - f_{FD,2}$) will flow from left to right while the others will flow from right to left (blue region of $f_{FD,1} - f_{FD,2}$). Consequently, there would be significant thermoelectricity generated if there is an abrupt change in the density of states $D(E)$ and if the absolute value of $D(E)$ is large near the Fermi level. In addition, for a typical conduction band (n-type semiconductor) as shown in Figure 3(b), there will be more electrons flowing from the hot contact to the cold one owing to the increased $D(E)$ at higher E, thereby causing a tendency of electron accumulation at the cold contact. As a result, the hot contact will work as the cathode with a higher voltage than the cold contact (anode). Based on the definition of the Seebeck coefficient,

$$V_{output} = -S\Delta T, \quad (12)$$

the Seebeck coefficient of n-type TE materials is thus negative. Similar analysis can be conducted on p-type TE materials to obtain a positive S.

Quantitatively, the Mott formula describes the Seebeck coefficient for a metal or degenerate semiconductor as [46]

$$\begin{aligned} S &= \frac{\pi^2 k_B^2}{3e} T \left\{ \frac{d\left[\ln\left(\sigma(E)\right)\right]}{dE} \right\}_{E=E_F} \\ &= \frac{\pi^2 k_B^2}{3e} T \left\{ \frac{1}{n}\frac{dn(E)}{dE} + \frac{1}{\mu_m}\frac{d\mu_m(E)}{dE} \right\}_{E=E_F}, \end{aligned} \quad (13)$$

in which E_F is the Fermi level, n is carrier density, and μ_m is carrier mobility. Therefore, a larger S can be achieved by increasing the energy dependence of $n(E)$ or, equivalently, the curvature of the density of states $D(E)$ in Figure 3, near E_F (usually equivalent to the chemical potential μ) by the so-called band engineering. This can be achieved by increasing the band degeneracy through alloying [11, 47, 48], introducing resonance levels through impurity doping [6, 49] or inducing quantum confinement through superlattice or low-dimensional structures [26, 27]. It will be demonstrated in this review that carbon-based nanomaterials can be physically or chemically engineered into various structures with substantially different electronic band structures from their bulk counterparts, which could sometimes lead to enhanced S. In addition to band engineering, S can also be increased by increasing the energy dependence of carrier mobility $\mu_m(E)$ through energy filtering.

2.2. Lattice Thermal Transport. To achieve efficient TE energy conversion, a low thermal conductivity is required to minimize the heat loss from the hot to the cold side, which could otherwise be used for generating electricity in the generator mode. Such effect is reflected in the expression for ZT in (4), in which the thermal conductivity is the denominator. Since κ_e and σ are tightly coupled by the Wiedemann-Franz

law (3), reducing the lattice thermal conductivity κ_L is a straightforward strategy for reducing the heat loss, as revealed by (4). In crystals of which the lattice has a well-defined periodicity, lattice heat transfer occurs by collective atomic vibrations, or phonons. Differently, locons, diffusons, and propagons are believed to account for the thermal transport in amorphous materials [50], which do not have a well-defined unit cell. Here, we will provide a brief introduction to phonon transport in TE materials, which are mostly semiconductors, semimetals, or alloys.

Similar to (6) for σ, the lattice thermal conductivity can be calculated through

$$\kappa_L = \sum_{\lambda} c_\lambda v_\lambda^2 \tau_\lambda, \tag{14}$$

which also originates from BTE. In this equation, λ denotes phonon mode, c is the specific heat of the phonon mode, v is the phonon group velocity, and τ is the phonon relaxation time or lifetime, of which the inverse is called the phonon scattering rate (τ^{-1}). The group velocity of phonons can be manipulated through strain or creating phononic crystals, for example, periodic holey structures and superlattices. The formation of phononic crystals usually creates large phonon bandgaps and flattens phonon dispersion curves, leading to reduced group velocity and thus reduced κ_L. The phonon relaxation time τ can be affected by various mechanisms, of which the overall effect is usually approximated by Matthiessen's rule as

$$\begin{aligned}\tau^{-1} = {} & \tau_U^{-1} + \tau_N^{-1} + \tau_e^{-1} + \tau_m^{-1} + \tau_{GB}^{-1} + \tau_{NP}^{-1} + \tau_D^{-1} + \tau_S^{-1} \\ & + \tau_{PD}^{-1} + \tau_{DL}^{-1} + \cdots,\end{aligned} \tag{15}$$

in which τ_U, τ_N, τ_e, τ_m, τ_{GB}, τ_{NP}, τ_D, τ_S, τ_{PD}, and τ_{DL} denote the relaxation time limited by scatterings through Umklapp processes, normal processes, electrons [51, 52], magnons [53], grain boundaries, nanoprecipitates, dislocations, strain fields, point defects, and displacement layers, respectively. In many ingenious designs of TE materials or structures, several mechanisms for phonon scatterings are usually combined to achieve largest possible reduction in phonon transport. The so-called all-scale hierarchical architecture [47, 54] is one such design that incorporates most of the above phonon scattering mechanisms into one single material, which has demonstrated ultralow κ_L and one of the highest values of ZT reported so far. Recently, phonon localization [33, 34, 55, 56] is also being investigated as an additional effective mechanism for suppressing phonon transport in materials, which can be combined with phonon scattering mechanisms to achieve ultralow κ_L [57]. As shown in Figure 2, several carbon-based nanomaterials like graphene and carbon nanotube have high thermal conductivity, which is detrimental for TE applications. Reducing κ_L of these materials is thus one major issue for realizing efficient TE energy conversion with these materials.

It is worth noting that common strategies utilizing nanotechnology to reduce the lattice thermal conductivity usually deteriorate electrical conductivity simultaneously, which undermines the benefit of nanoengineering. Fortunately, the scattering mechanisms mentioned in (15) usually affect electron and phonon transport by different degrees. For example, Figure 4 shows the cumulative electrical conductivity and lattice thermal conductivity as a function of electron or phonon mean-free-path for Si [58] and PbTe [59], which approximately quantifies how σ or κ_L can be truncated by a specific material size. Evidently, a specific material or grain size truncates σ or κ_L by different degrees and there are regions in which κ_L is substantially reduced while σ is much less affected, which could be beneficial for the ZT. Take Si, for example; the normalized cumulative thermal conductivity is approximately 30% for the phonon mean-free-path of 100-nm (Figure 4). This means a nanosized Si crystal with a critical dimension of 100 nm only has approximately 30% of κ_L of bulk Si. In contrast, the cumulative electrical conductivity is still 100% for both carrier concentrations of 10^{16} cm^{-3} and 10^{19} cm^{-3}, which means that σ of 100 nm Si is almost the same as its bulk-limit value. In fact, the normalized cumulative conductivity curves are affected by several extrinsic or intrinsic factors, such as temperature and carrier concentration. As shown in Figure 4, different carrier concentrations (10^{16} cm^{-3} and 10^{19} cm^{-3}) can lead to significant shift and distortion to the cumulative electrical conductivity curves, determined by the details of electronic band structure near the corresponding Fermi level.

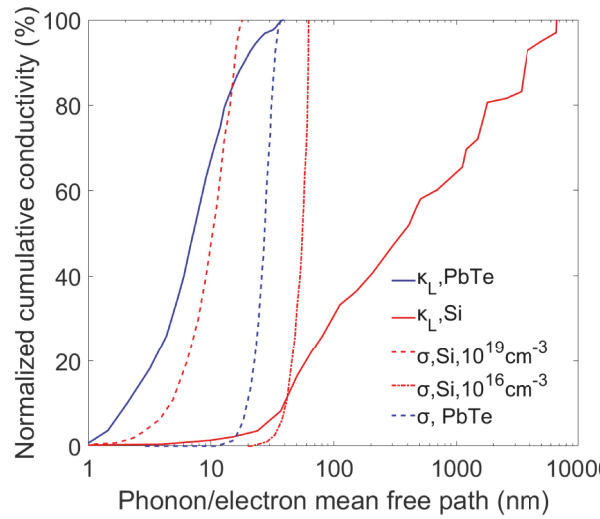

Figure 4: Normalized cumulative conductivity (at 300 K), i.e., electrical conductivity σ and lattice thermal conductivity κ_L, with respect to the corresponding electron or phonon mean-free-path for Si [58] and PbTe [59]. The normalized cumulative conductivity quantifies how material size can affect the conductivity of nanomaterials, i.e., the percentage of conductivity remaining (vertical axis) for a specific size (horizontal axis) of nanomaterial due to the truncation of mean-free-path by materials' boundaries.

2.3. Mechanical Properties. The majority of the research efforts in the area of thermoelectrics have been focused on enhancing the TE properties. The understanding of the mechanical properties and failure mechanisms is still scarce but critical for the robustness and performance of

TE materials and devices. Under a temperature gradient or cyclic working conditions, thermal stress will accumulate inside TE materials. The mismatch between the thermal expansion coefficients of the TE materials and electrodes in the TE device will also generate stresses at the interface. These thermal stresses will cause the degradation and failure of TE materials and even the entire device, imposing a critical demand of excellent mechanical properties of TE materials for vast commercialization. To survive extreme temperature, cyclic loading, and thermal mismatch, capable TE materials need to have both high strength and high toughness, to ensure that the materials are hard to deform and hard to fracture. The strength and ductility of the materials are controlled by the difficulty to move the carriers of plastic deformation, such as dislocations, twin boundaries, and grain boundaries, in materials. Toughness is controlled by the ability of materials to survive cleavage fracture. For engineering applications, robust devices need components made from materials with high strength, suitable ductility, and high toughness. All these properties are controlled by the material microstructure, which is the complex network of materials defects, e.g., dislocations, twin boundaries, and grain boundaries. Therefore, microstructure engineering has been used extensively in metal, alloys, and ceramics to enhance the mechanical properties of materials [60–62].

The best inorganic TE materials are mostly semiconductors, which are usually brittle and prone to fracture, except for certain ductile alloys with poorer TE performance. Many recent studies focused on investigating the mechanical properties of TE materials. For instance, Snyder et al. used quantum-mechanical simulations to predict the ideal shear strength of La_3Te_4, an n-type high-temperature TE material [63], in which they proposed using partial substitutions of La by Ce or by Pr to improve the shear strength. He et al. used nanoindentation and atomic force microscopy to characterize the hardness and elastic modulus of several TE materials, including half-Heusler, skutterudites, Bi_2Te_3, SiGe alloys, and PbSe [64], in which p-type half-Heusler exhibited higher hardness and modulus and was found to be less brittle than other materials tested.

Similar to the microstructure engineering strategies used in metals and alloys, there have been extensive recent efforts devoted to improving the strength, ductility, and toughness of inorganic TE materials. In low-strength TE materials, such as GaAs, ZnSe, Bi_2Te_3, and InSb, several studies focused on engineering the material microstructure to increase the mechanical strength. For example, Snyder et al. introduced nanosized twin boundaries into InSb and found an 11% increase in shear strength [65]. In another work, Snyder et al. found that spark plasma sintering (SPS) reduced the grain size of $(Bi,Sb)_2Te_3$ compared to the samples processed with the traditional zone-melting method. The SPS-processed samples exhibited higher strength and higher fracture toughness [66].

In fact, microstructure engineering could lead to simultaneously improved TE and mechanical properties of materials. For instance, Zhu et al. used hot deformation to introduce material defects, such as dislocations, point defects, and grain boundaries, into p-type $(Bi,Sb)_2Te_3$. Those defects are well known to harden materials [67–69]. Moreover, they can also modify the carrier concentration and reduce the thermal conductivity, potentially leading to improved TE performance. Similarly, both reduced thermal conductivity and increased Vickers microhardness were observed for GeSbTe alloys, which were attributed to the coexistence of various defects, including domain boundaries, twin boundaries, precipitates, and solid solution point defects, in the samples [70]. Very recently, high room-temperature ductility was reported for an inorganic semiconductor: α-Ag_2S [71]. The low-energy barrier to move dislocations ensures that α-Ag_2S can sustain large plastic deformation before final failure. This finding could inspire possible alloying strategies to assist plastic deformation in inorganic TE materials, in order to increase ductility and avoid cleavage fracture.

Finally, it is worth noting that, in contrast to traditional brittle inorganic semiconductors, carbon-based TE materials, such as graphene and carbon nanotubes and polymer-based composites, usually have much higher mechanical flexibility or higher fracture toughness. Therefore, carbon-based materials and composites could be outstanding candidates for mechanically robust TE materials.

3. Carbon Allotropes as Thermoelectric Materials

Carbon atom has four valence electrons, allowing it to form four covalent bonds. Its capability of forming sp, sp^2, and sp^3 bonds renders a large variety of carbon allotropes. Notably, diamond and graphite are the most well-known 3D allotropes of carbon, while graphene, carbon nanotube (CNT), and fullerene are the most widely studied 2D, 1D (or quasi-1D), and 0D allotropes. There are also other forms of carbon allotropes, in particular, amorphous carbon, such as diamond-like-carbon. As shown in Figure 2, the thermal conductivity of these carbon allotropes can differ by 5 orders of magnitude, varying from 0.01 W/m-K for amorphous carbon to more than 3,000 W/m-K for graphene and CNT. The thermal conductivities of diamond and those of the inplane direction of graphene and graphite are among the highest measured values reported so far, which renders them useful for various applications that need fast heat dissipation, for example, thermal management of electronic and photonic devices [36, 37]. Nonetheless, high thermal conductivity is deteriorating for TE applications, which prevents the application of these materials as TE materials in their original forms. Fortunately, there are still certain unique properties of some of these allotropes rendering them promising as TE materials after modification of structure or careful design of the configuration of the TE devices. For example, graphene, a stand-alone single layer of graphite has a 2D lattice of carbon atoms connected by sp^2 bonds. Its unique 2D structure endows graphene with Dirac-cone-like linear electronic bands, which lead to excellent charge transport properties. For instance, an ultrahigh mobility exceeding 2×10^5 cm^2/V-S at electron densities of ~2×10^{11} cm^{-2} was measured for suspended graphene [72] at ~5 K. Despite the high mobility, however, the low Seebeck coefficient and high κ_L of intrinsic

graphene prevent it from being a useful TE material in its original form. In this section, we aim to provide a review of TE materials based on carbon allotropes and highlight strategies for effectively improving the TE properties of these materials.

3.1. Graphene and Graphene Nanoribbons. Graphene is a zero-bandgap semimetal, of which the valence band and conduction band meet at the Dirac points. The gapless band structure and the linear dispersion near the Fermi level in bulk pristine graphene lead to a small Seebeck coefficient S owing to the cancellation of the contributions from electrons and holes. Nonetheless, notable S can be obtained by moving the Fermi level away from the Dirac points through doping or modifying the band structures through band engineering. For example, Ouyang and Guo demonstrated using nonequilibrium Green's function (NEGF) approach that a nontrivial $|S|$ of around 80 μV/K can be achieved through electron or hole doping or, in other words, by moving the Fermi level away from the Dirac point [73]. The authors also found that, by cutting bulk graphene into graphene nanoribbons (GNR), of which the two most common structures (armchair GNR and zigzag GNR) are shown in Figure 5(a), the maximally achievable S can be dramatically increased to 4,000 μV/K owing to a modification in band structure. Even though this high value of S is only a theoretical limit, it is much higher than that of most TE materials studied so far, indicating the feasibility of nanoengineering graphene into excellent TE materials.

A significant drawback of graphene as a TE material is its high κ_L, as shown in Figure 2. However, there exist various strategies for reducing κ_L of graphene through nanoengineering, for example, by introducing isotopes [76–78], vacancies [79–82], nanoholes [83, 84], dislocations, or grain boundaries. Cutting graphene into graphene nanoribbon was also found to be effective in reducing its κ_L, which arises from a combination of enhanced phonon-boundary scattering [85–87] and phonon-edge localization [37, 55, 56].

Anno et al. studied the effect of structural defects on the TE performance of bulk graphene [74]. Specifically, they adopted oxygen plasma treatment to introduce controlled structural defects by changing the plasma intensity and treatment time. Graphene with few defects was found to exhibit almost a constant ZT value when the defect concentration is increased, as both the power factor and thermal conductivity decrease due to the introduced defects (Figure 5(b)). However, as the defect density further increases beyond a critical value, the decrease in thermal conductivity outweighs the impact of the reduction in power factor, leading to increased ZT. As shown in Figure 5(b), ZT can be enhanced to 2.6 times of the ZT of pristine graphene.

In a theoretical study by Yeo et al., uniaxial tensile strain was found to enhance the ZT of both n-type and p-type armchair GNR (aGNR) due to the modification of electronic and phonon band structures [88]. They found that aGNRs with $N = 3p$ and $N = 3p + 2$, where N is the number of carbon dimers along the width direction and p is an integer, can have increased ZT. The increased ZT of $N = 3p$ cases are caused by the enhancement in electron transmission around the valence and conduction band edges, while the increased ZT of $N = 3p + 2$ cases arise from the suppression of unfavorable bipolar transport by the enlarged band gap. It is worth mentioning that phonon localization in GNRs has been found to account for an additional part of reduced κ_L other than phonon-edge scattering. As shown in Figures 5(c)–5(e), there are considerable amounts of phonon modes localized at GNR edges, which significantly reduces κ_L together with the effect of phonon-edge scatterings [56].

Sevinçli et al. have shown that edge disorder in the form of erosion (Figure 5(f)), or roughness, can reduce the thermal conductivity of zigzag GNRs (zGNR) significantly while leaving the originally high electrical conductivity rather unaffected [75]. The reason for the reduced thermal conductivity lies in the fact that edge disorders can suppress the phonon transmission at almost all energy levels, as shown in Figure 5(g). On the other hand, electron transmission is also suppressed but not as much as that of phonon, as displayed by Figure 5(h), because higher-energy electrons are well dispersed within the ribbon and thus charge transmission is barely affected. As a consequence of the much stronger reduction in phonon transmission than electron's, a room-temperature ZT of 4 was predicted for edge-disordered zGNR, which was much higher than that of the pristine one.

3.2. Graphene Nanomesh. In the above sections, we have discussed graphene and GNR structures with enhanced TE properties through a reduction in κ_L or a modification of the electronic band structure. Graphene is a versatile structure that can be engineered into various forms and achieve diverse properties. In 2010, Bai et al. fabricated single- and few-layer graphene layers with a high density array of nanoholes, which they named graphene nanomesh (GNM) [91]. A typical microscopy image [90] of GNM is shown in Figure 6(a). In fact, GNM can be viewed as a phononic crystal (PnC), which typically refers to synthetic metamaterials formed by periodic variation of the phononic (mainly acoustic) properties of the original material(s). The most notable feature of PnCs is the creation of phononic bandgaps, which leads to new phonon transport properties, for instance, reduced κ_L [84, 92, 93] and coherent phonon transport [94]. It is worth mentioning that the reduced κ_L is commonly attributed to decreased phonon group velocities due to the zone-folding effect [95], which represents the phenomenon that periodic arrangement of microfeatures in a material modifies the phonon band structure in a way as if the phonon bands are folded into the first Brilloin zone. The immediate effect of such band folding is enlarged bandgap and reduced phonon group velocities. Owing to the similarity in structures, GNM is expected to share some similar characteristics as the phononic crystals of other materials, e.g., SnSe and silicon [84, 92–94, 96]. Such special structure of graphene has triggered a series of studies regarding the thermal and TE transport in this structure.

Hu and Maroudas conducted molecular dynamics (MD) simulations using the adaptive interatomic reactive empirical bond-order (AIREBO) potential to determine the effect of pore morphology and pore edge passivation on thermal conductivity of GNMs with circular and elliptical holes [89]. The authors found that the thermal conductivity of GNM is

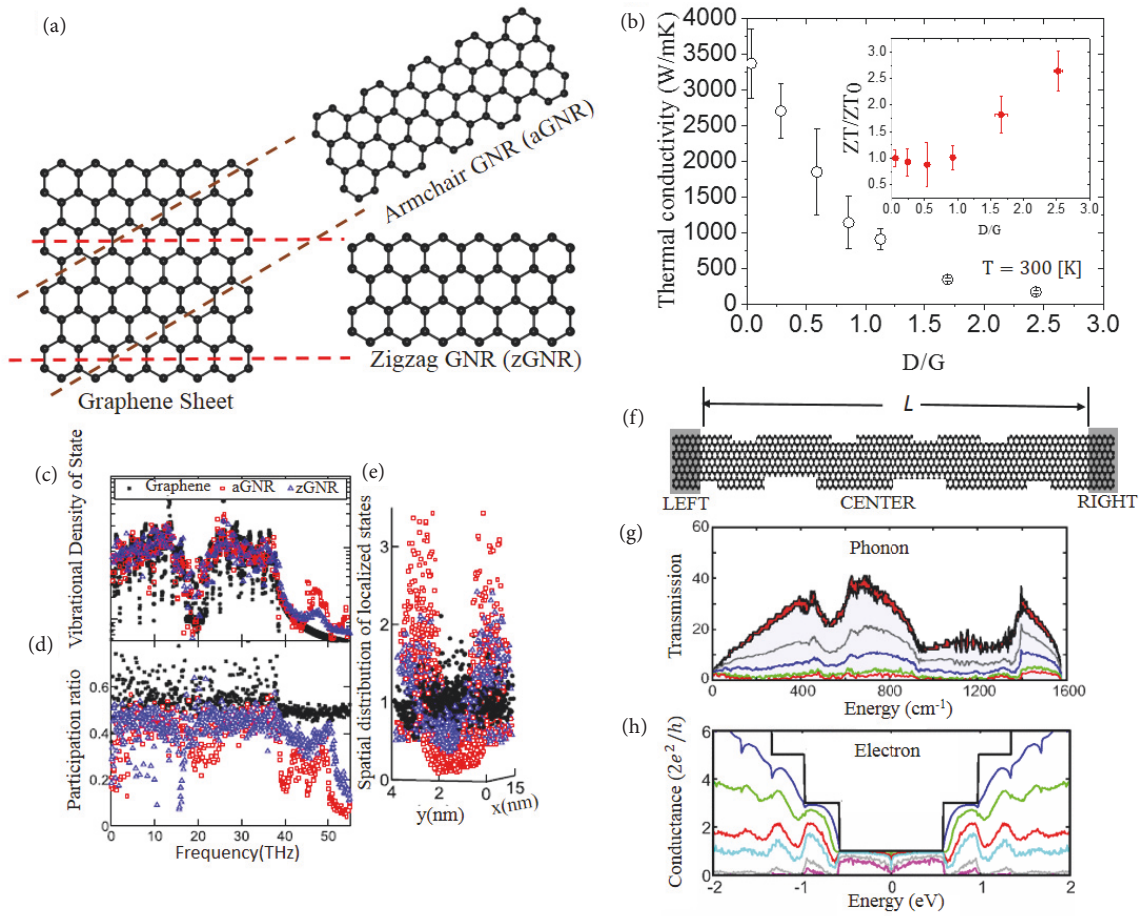

FIGURE 5: (a) Schematics of the lattice structures of graphene and graphene nanoribbon. (b) Defect density dependence of the thermal conductivity of suspended graphene [74]. The inset shows ZT of defected graphene normalized by that of pristine graphene with respect to D/G at room temperature. D/G ratio is used in Raman spectroscopy to denote the defect density. (c)–(e) The vibrational density of states, phonon participation ratio, and spatial distribution of localized modes in bulk graphene, aGNR, and zGNR [56]. In particular, the height in (e) corresponds to the magnitude of localization at that position. (f) Schematic of edge-disordered zGNR of length L sandwiched between two semiinfinite pristine zGNRs. ((g) and (h)) Phonon transmission and electron conductance for pristine and edge-disordered zGNR with a width of 20 dimer lines, respectively [75]. Panels (c)–(h) are reproduced with permission [56, 75].

related to its neck width as $\kappa \sim \kappa_0 \exp(W_{neck}/L)$, where κ_0 is the thermal conductivity of pristine bulk graphene, W_{neck} is the neck width (as illustrated in Figure 6(b)), and L is a constant with a length unit. Another important finding of their study is that pore edge passivation has negligible impact on κ_L of GNMs, owing to the already strong phonon-edge scattering that prevails the passivation effect. They also found negligible effect of the arrangement of the location of nanopores on κ_L. Moreover, unlike the circular one, elliptical nanoholes in GNM lead to an anisotropic κ_L and such anisotropy increases as the aspect ratio of the elliptical hole increases, further demonstrating the strong controllability of thermal transport in GNMs.

Similar to Hu and Maroudas' study, Sadeghi et al. demonstrated that the ZT of GNR can be increased by introducing nanopores to the basal plane of single layer or bilayer GNRs [97]. They demonstrated, using the density functional theory (DFT)-aided NEGF method, that bilayer GNRs with nanopores can have a ZT as high as 2.45. For monolayer graphene, they also demonstrated a substantial increase from 0.01 to 0.5 at room temperature. In addition to the improved ZT, bilayer GNR containing nanopores is also believed to be structurally and thermodynamically more stable than monolayer porous GNR, which has a higher chance to be used in practical applications. The effect of nanoholes on TE transport in GNR can be understood in the following manner. On one hand, nanoholes can hinder phonon transport significantly through phonon scattering. Though not mentioned in [97], one should also expect significant phonon localization [55, 56] near the edges of the nanoholes, as confirmed by Feng and Ruan [83], no matter whether they are terminated with hydrogen or not. On the other hand, as revealed by Sadeghi et al., the nanoholes suppress the electron transmission far above or far below the

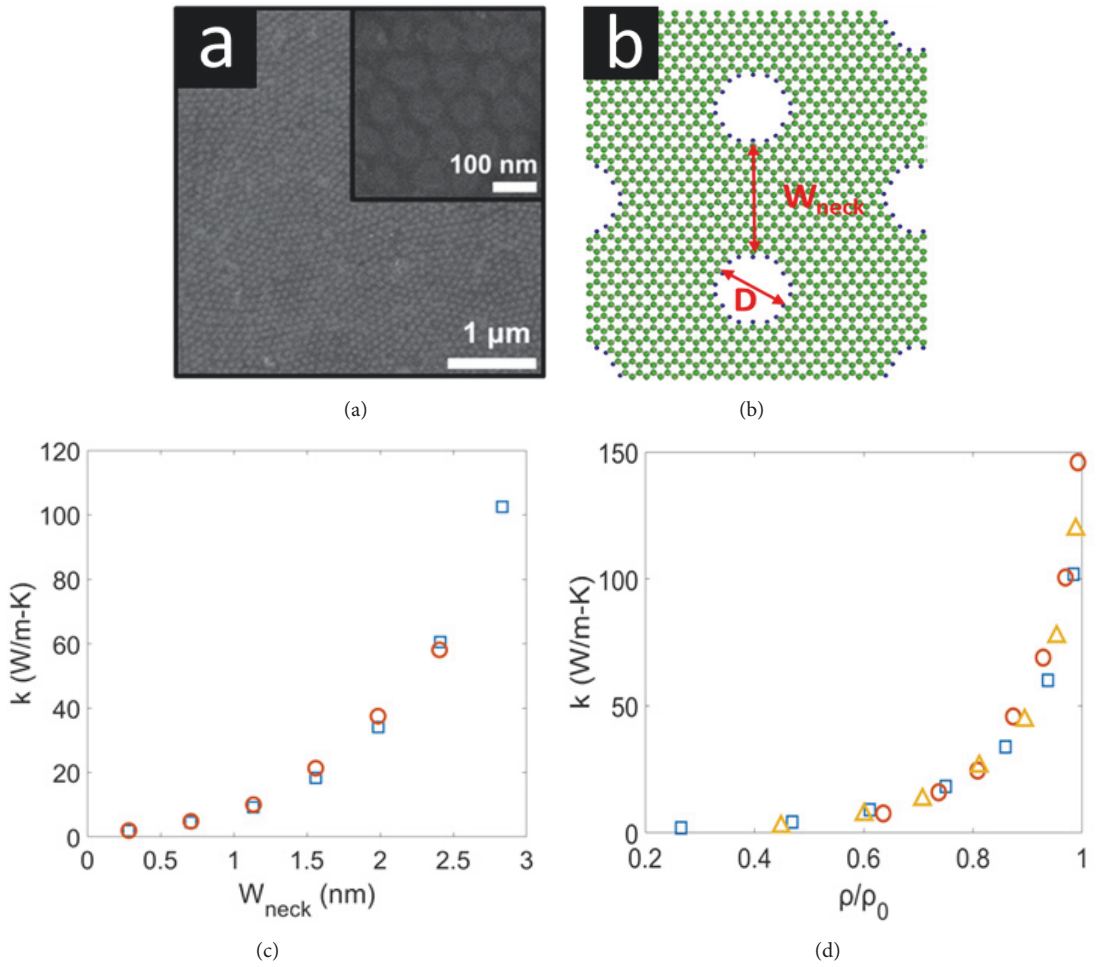

FIGURE 6: (a) Field-emission scanning electron microscopy image of graphene nanomesh. (b) Atomic structure of GNM, in which W_{neck} and D are the neck width and diameter of the holes, respectively. (c) The thermal conductivity κ as a function of the neck width W_{neck} [89]. (d) The thermal conductivity κ of GNMs as a function of the scaled density, $\rho/\rho 0$, with circular pores arranged in hexagonal (squares), honeycomb (circles) and square (triangles) lattices [89]. Panels (a) and (b) are reproduced with permission [89, 90].

Fermi energy, but the high transmission in the vicinity of Fermi level is preserved [97]. The overall effect of significantly reduced κ_L while less reduced σ is an enhancement in ZT.

There are also other explanations for the substantially decreased κ_L of GNM compared to pristine graphene. M. Yarifard et al., using equilibrium MD simulations combined with the Green-Kubo method, have demonstrated that the reduced thermal conductivity stems from the phonon caging effect [98]. Specifically, phonons are trapped in cages between the nanoholes and the effective group velocity of phonons is also reduced. This hypothesis was seemingly formed based on the phonon band folding mechanism [84, 92] as well as Hao et al. Monte Carlo phonon transport simulations [99]. Recently, Feng and Ruan conducted MD simulations and spectral energy density analysis to investigate phonon transport in GNMs, for which they found a 200-fold lower κ_L than corresponding GNRs with the same (neck) width and boundary-to-area ratio [83]. The ultralow κ_L of GNMs is attributed to the localization of phonons in the vicinity of the nanopores, as evidenced by the phonon participation ratio and backscattering of phonons.

Finally, it is worth mentioning that the electrical conductivity of GNM is found to be comparable to that in rectangular-shape GNRs with the same width [91, 100, 101]. The minimally affected electrical conductivity along with substantially reduced κ_L renders GNMs promising as TE materials.

3.3. Graphene Nanowiggle. In addition to the simplest form of GNR, other shapes of GNR or related structures have also been studied for their TE properties. Connecting same or different types of GNRs into a chain or quasi-1D superlattice is one of the most studied strategies for achieving better ZT properties. For instance, 1D wiggle-like GNR, or graphene nanowiggle (GNW), has been synthesized with atomistic precision using a bottom-up technique [102], of which the microscopy image is shown in Figure 7(a) [103] and the schematic atomic structure is shown in Figure 7(b).

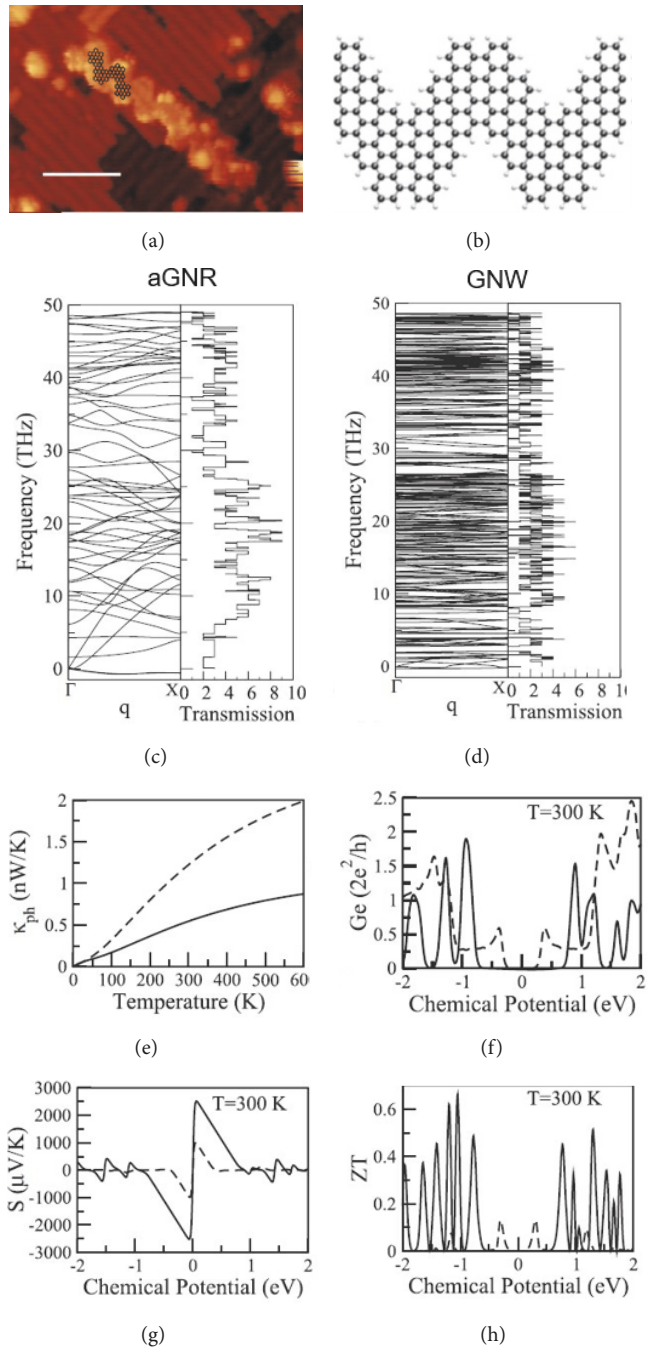

Figure 7: (a) Scanning tunneling microscopy image of graphene nanowiggle. (b) Atomic structure of GNW. ((c) and (d)) Phonon dispersion relations and transmission functions of aGNR and its GNW counterpart. (e) Thermal conductance as a function of temperature for aGNR and the GNW shown in panel (b). (f)–(h) Electrical conductance G_e, Seebeck coefficient S, and TE figure-of-merit ZT as a function of chemical potential at room temperature for aGNR and GNW. In panels (e)–(h), solid lines denote GNW and dashed lines denote the corresponding aGNR. All panels are reproduced with permission [103, 104].

Such GNW structure can be viewed as periodic repetitions of graphene nanoribbon junctions. This breakthrough has sparked a series of investigations of various physical properties of GNW, including TE properties. The corresponding structure is also referred to as kinked GNR, mixed GNR, or chevron type GNR in some other studies. The enhanced TE properties of this type of GNR arise from the modified band structure as well as added obstacles to phonon transport.

Huang et al. used a Landauer-based ballistic transport model to study the GNW structure (referred to as kinked GNR in their work) [105], in which armchair GNR and zigzag GNR are connected into a twisted, long chain. They found

that symmetry breaking at the kinks causes extensive phonon scatterings and hence a reduced lattice thermal conductivity κ_L. They also found that the ZT of kinked aGNR can be twice as high as that of straight aGNRs. Besides, unlike the metallic behavior of straight zGNRs (ZT~0), kinked zGNRs show broadening of the bandgaps owing to quantum confinement and thus exhibit semiconductor-like behaviors. As a result, a tangible ZT can be observed. Mazzamuto et al. also studied similar structures, which are referred to as mixed GNR in their work [106]. They used the NEGF method to demonstrate that mixed GNRs consisting of alternate layer of zigzag and armchair sections can show a ZT approaching or even higher than unity, which is much better than pure zGNRs or aGNRs. This enhancement in ZT stems from two effects: first, the mismatch of phonon spectra between armchair and zigzag GNRs causes very low phonon thermal conductance; second, resonant tunneling of electrons allows efficient transmission of electrons across the structure. Similar conclusions regarding the reasons for reduced thermal conductance and less affected electrical conductance were drawn in Liang et al. study (Figures 7(c)–7(h)), in which they used DFT calculations along with the NEGF approach [104]. Moreover, Liang et al. found that GNWs exhibit less dispersive phonon branches compared to GNR and lower values of phonon transmission function, as shown in Figures 7(c) and 7(d), which reduces κ_L. In addition, GNW can be considered as a multibarrier system which experiences strong oscillation of electrical conductance and thermopower due to resonant tunneling effect. The highest room-temperature ZT among all the structures considered in their work is 0.79. Similarly, Chen et al. [107] also predicted a high ZT of 0.63 for GNWs, which suggests the potential usefulness of the GNW structure for thermoelectrics.

Sevinçli et al. extended the research on GNW structure even further by looking into the effect of scattered and clustered ^{14}C isotopes on its TE properties [108]. Specifically, they found, based on atomistic Green's function calculations for both electrons and phonons, that GNWs containing isotope clusters can have a 98.8% lower thermal conductance than the corresponding straight GNR. Such isotopically modified GNW is thus advantageous over isotopically pure GNWs, which show κ_L only 69% lower than that of straight GNRs. As a result, the ZT of isotopically modified GNW can be as high as 3.25 at 800 K. Similar to previous studies [104–106], the reduced κ_L is attributed to the reduced phonon group velocity caused by the formation of minigaps in the phonon band structure.

3.4. Carbon Nanotube. Carbon nanotube, commonly referred to as CNT, is another common form of carbon allotropes that has been studied extensively for its TE properties [5, 109]. In Figure 8, we summarize some notable values of the Seebeck coefficient and electrical conductivity of CNTs measured recently [110–127]. Obviously, the TE properties of CNT can be tuned in a wide range, of which the prominent strategies will be discussed in this subsection.

CNTs can have various forms: single-walled (SWCNT), double-walled (DWCNT), and multiwalled (MWCNT), which can be viewed as a rolled single-, double-, or multilayer GNR, respectively. Similar to graphene, carbon atoms in CNTs are sp^2-bonded and the resulting π electrons endow certain structures of CNT with high electrical conductivity (up to 10^6 S/m) [128, 129]. Besides, the low mass of carbon atoms, strong C-C covalent bonds, and low anharmonicity of the lattice render CNT a high-κ_L material similar to graphene [37]. Indeed, theoretical models [130–132] and numerical simulations [133] have predicted a divergent κ_L when the length of 1D and 2D crystals increases. Recent experiments on millimeter-long SWCNTs [134] and up to 9 μm long single-layer graphene [135] have demonstrated divergent κ_L, with a maximum room-temperature κ_L of 8,640 W/m-K and 1,813 $\pm$ 111 W/m-K, respectively, even though there are concerns regarding the existence of radiative heat loss during the measurement on SWCNTs [136]. Such high κ_L, however, renders CNT and graphene inappropriate as TE materials in their raw forms. In this subsection, we will review recent progress in TE materials in which CNT serves as the primary transport phase. We will discuss composites composed of CNT and other organic/inorganic materials in Section 4. The readers are also recommended to read the comprehensive review on CNT-based TE materials and devices by Blackburn et al. [5] for more details.

CNT, especially SWCNT, is a unique system of which the carrier density and Fermi level can be modified using charge transfer doping, owing to the extremely large surface-to-volume ratio of CNTs and the sensitivity of the π electrons to surface-mediated redox reactions. In particular, even physisorbed molecules can affect the carrier density significantly. Sumanasekera et al. have experimentally shown that the TE properties of air-exposed SWCNTs (physisorbed with oxygen molecules) are completely different from those of intrinsic (degased) ones [137]. Specifically, oxygen saturated SWCNTs were found to exhibit strong p-type TE behavior whereas the degased ones exhibited n-type TE behavior. This swing in the Seebeck coefficient stems from the charge transfer between the physisorbed O_2 and SWCNTs. Moreover, it was observed that the collision between the wall of SWCNT and N_2 or even inert gases like helium can modify the electrical conductivity and the Seebeck coefficient notably. Regarding such air stability issue (i.e., physisorption of O_2 transforms SWCNT into p-type or SWCNT with physisorbed O_2 transforms into n-type in vacuum), nitrogen [138] and boron [139] doping are found to be effective in rendering the CNTs as permanent (stable in air and vacuum) n-type or p-type materials, respectively.

Other than doping, applying an external voltage can also modify the Fermi level directly. Kim et al. have conducted a series of experiments on CNT-based TE devices and demonstrated that TE transport can be readily tuned by the applied gate voltage [140, 141]. They also observed a room-temperature Seebeck coefficient of 80 μV/K in individual MWCNT [141]. Later, in 2005, Yu et al. measured a value of 42 μV/K for individual SWCNTs [142], which is one order of magnitude higher than that of graphite or typical metals, indicating CNTs' potential for TE applications. However, the high κ_L of CNTs still limits the efficiency of CNT-based TE devices.

Tan et al., through a combination of nonequilibrium MD simulations and NEGF simulations, have shown that the ZT

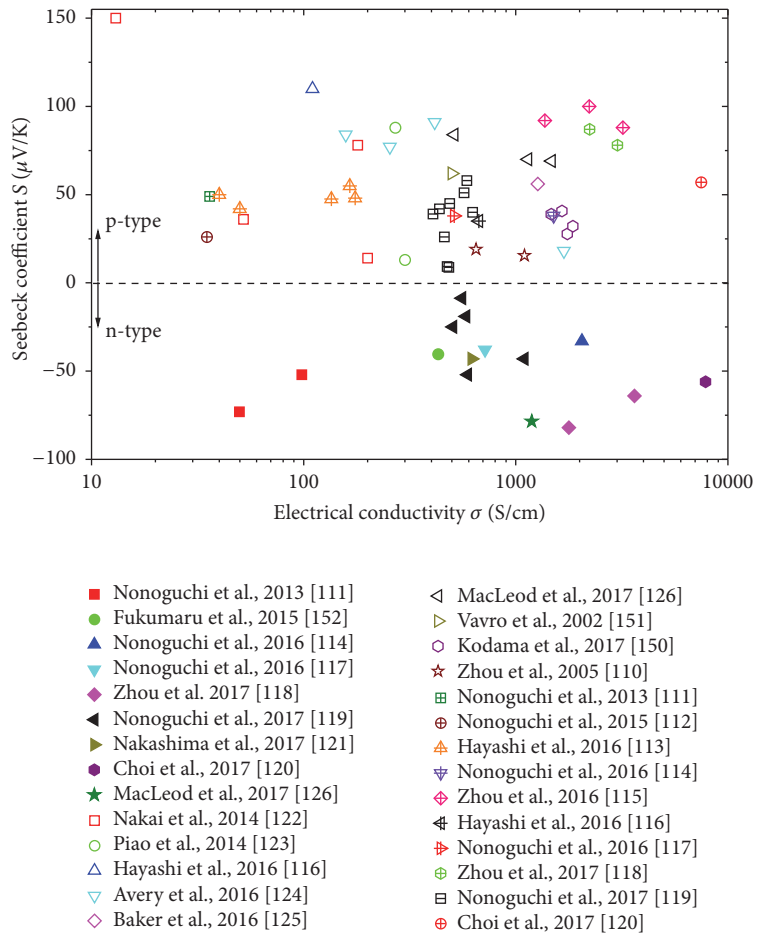

Figure 8: Seebeck coefficient and electrical conductivity of SWCNT-based TE materials measured in previous studies.

of CNT can be enhanced by optimizing the carrier concentration at certain operating temperatures [143]. Consistent with previous studies [144, 145], Tan et al. concluded that the κ_L of both zigzag and chiral CNTs decreases as the tube diameter increases due to decrease in average group velocity and increase in Umklapp scatterings. Chiral tubes possess lower κ_L than the zigzag counterparts due to more frequent Umklapp scatterings. The Seebeck coefficient S is maximized at $\mu \approx \pm k_B T$ away from the band edges, while it vanishes near the bandgap edge. The peaks of ZT near the Fermi level indicate that appropriate doping, which controls the location of chemical potential, can maximize the ZT of CNTs. Based on this hypothesis, Tan et al. demonstrated a maximum ZT of 0.9-1.1 at different μ's for different types of SWCNTs. In addition, Tan et al. emphasized that randomly distributed isotopes (^{13}C) can further reduce κ_L of CNT without affecting its electronic properties, thus increasing its ZT. They predicted a highest ZT of 4.2 at T = 800 K for isotopically doped CNT. An increase in ZT by isoelectronic impurities (Si) and hydrogen adsorption was also observed owing to the similar reason. Even though the predicted maximum value of ZT (around 4) seems too optimistic, this work reveals the potential of CNT as outstanding TE materials.

In fact, CNTs are often produced as bundles or networks and many applications need such bulk-form CNTs rather than isolated ones. Therefore, extensive research efforts have been devoted to exploring TE transport in bulk CNTs, such as films, fibers, or bundles of CNTs. Prasher et al. conducted both experimental and computational investigations on thermal transport and TE properties of 3D random networks of SWCNTs and MWCNTs, which were referred to as CNT beds [146]. The CNT beds were constructed by pressing commercially available CNTs at various pressures (138-621 kPa). They measured an ultralow thermal conductivity in the range of 0.1-0.2 W/m-K at room temperature, which is even lower than isotropic polymers (~0.2 W/m-K). They attributed the ultralow thermal conductivity to the extensive number of contacts between individual CNTs, as evidenced by their MD simulations and atomistic Green's function calculations. They also measured the Seebeck coefficient S, which was found to be comparable to isolated SWCNTs but largely depends on the diameter of the CNTs. They hypothesize that this is caused by the fact that larger-diameter CNTs have smaller band gaps (approaching the zero-band-gap graphene limit), which reduces S. The authors estimated that the ZT of CNT beds can be as high as ~0.2 (orders of magnitude higher than that

of isolated SWCNT), even though no electrical conductivity measurement was directly performed.

Miao et al. studied the TE performance of ultralong DWCNT bundles [147], which were separated from purified DWCNT films. The measured thermal conductivities of the bundle varied between 25 W/m-K and 40 W/m-K, which is much lower than that of individual DWCNTs (about 600 W/m-K [148]). The reduced thermal conductivity was attributed to three possible mechanisms: (1) low volume fraction of CNTs in the bundle; (2) intertube interactions, in the form of van der Waals force, suppressing phonon transport; (3) the existence of defects, impurities, and amorphous carbon. The 1st and 3rd factors are easier to understand, while the effect of intertube interaction on phonon transport in CNTs is not as straightforward but has been studied extensively. For instance, Aliev et al. attributed the reduced thermal conductivity in bundled CNTs and MWCNTs compared to individual SWCNTs to radiative heat loss in the radial direction of the CNT and quenching of phonon modes by intertube interaction [149]. Particularly, intertube interaction restricts the rotational and vibrational degree of freedom of confined nanotubes and thus leads to quenching of phonons and reduced thermal conductivity [149]. The reduction of phonon transport in such way indicates the opportunity for bundled CNTs as TE materials.

Attempts to reduce κ_L and hence increase ZT by introducing rattlers, e.g., C_{60} molecules, inside the hollow core of SWCNT or MWCNT, have been made [150, 151]. For example, in Vavro et al. pioneering work [151] in 2002, C_{60}-encapsulated SWCNTs were found to provide additional conductive paths for charge transport and increase phonon scattering. However, they found a Seebeck coefficient of 40 μV/K, which is lower than that of hollow SWCNTs (60 μV/K).

In 2015, Fukumaru et al. reported remarkable TE performance of cobaltocene-encapsulated SWCNTs (denoted as $CoCp_2$@SWCNTs) with a superior doping stability, resulting from the molecular shielding effect, compared to those doped on the outer surface of the tubes [152]. The synthesis procedure of $CoCp_2$@SWCNTs can be found elsewhere [153]. Free-standing $CoCp_2$@SWCNTs were bent to a radius of 3.5 mm for around 1,000 times without fracture, which confirms the flexibility of these structures under periodic loads. Regarding electrical properties, an increase in carrier density was observed when the $CoCp_2$ molecules were oxidized. Moreover, $CoCp_2$@SWCNTs, when exposed to air, demonstrated a stable n-type behavior (S = -41.8 μV/K) at 320 K. A ZT = 0.157 was achieved due to its high electrical conductivity and low thermal conductivity (~0.15 W/m-K) resulting from the high interfacial thermal resistance.

In a more recent work, Kodama et al. measured the TE performance of SWCNT bundles with encapsulated buckminsterfullerene (C_{60}) and endofullerenes ($Gd@C_{82}$ and $Er_2@C_{82}$), which were referred to as peapods [150]. The schematics of these structures are shown in Figure 9(a). It was found that the encapsulation can reduce the thermal conductivity by 35%-55% and enhance the Seebeck coefficient by approximately 40% (Figures 9(b) and 9(c)). As a result, the peapods exhibited 2-4 times higher ZT than that of hollow SWCNTs. Specifically, the reported ZT for hollow SWCNT and SWCNTs encapsulated with C_{60}, $Gd@C_{82}$, and $Er_2@C_{82}$ are 2.03×10^{-4}, 7.81×10^{-4}, 4.55×10^{-4}, and 8.45×10^{-4}, respectively. The lower thermal conductivity of encapsulated CNTs than hollow ones is attributed to the distortion of CNT and fullerenes caused by the local interaction between them, as confirmed by their MD simulations and transmission electron microscopy (TEM) analysis. Specifically, the local radial strains weaken the C-C bond in SWCNT, leading to softening of certain high-frequency acoustic phonon modes. The softened phonon modes have lower group velocity when the interaction between SWCNT and encapsulated fullerenes becomes stronger. The aforementioned quenching effect was also believed to cause the reduced thermal conductivity in the peapods [149].

3.5. Other Allotropes of Carbon. In addition to the well-known carbon allotropes, graphene, and CNT, other allotropes of carbon, for example, fullerene (C_{60}, C_{80}, etc.) and graphyne, have also been explored for their TE properties. Recent experimental and theoretical studies [154–157] of C_{60}-based TE devices have demonstrated C_{60} as a robust TE material, with a consistently negative S stemming from the broad lowest unoccupied molecular orbital (LUMO) level near the Fermi energy. However, the monotonic shape of LUMO makes it challenging to change the sign of S, rendering it necessary to explore the derivatives of fullerene for better TE performance. For instance, in the endohedral fullerene $Sc_3N@C_{80}$, the Sc_3N molecule in the fullerene cage not only creates a transmission resonance, which essentially suggests a possibly large S, but also affects the resonance energy and even the sign of S through its orientation relative to the cage. Recognizing such unique properties of $Sc_3N@C_{80}$, Rincón-García et al. demonstrated that an external pressure applied by the tip of scanning tunneling microscope onto the single molecule of $Sc_3N@C_{80}$ can tune the sign and magnitude of S effectively, with S varied between approximately -20 μV/K and 25 μV/K in their work [158].

It is worth noting that S of the fullerene-based molecular TE devices mentioned above is rather low (<50 μV/K) [154–158]. One of the key challenges in obtaining a high S in molecular junctions is accurately controlling the Fermi level to match the molecular energy level for transmission resonances. Regarding this issue, in 2017, Gehring et al. measured the TE properties of graphene-fullerene junctions [159], in which single-molecule C_{60} was used as the device and two graphene layers were used as leads, as shown in Figure 10(a). Their experiment showed that 1 to 2 orders of magnitude larger power factor can be obtained by tuning the gate voltage and the highest S obtained in their work was 460 μV/K, much higher than previous studies on C_{60}-based molecular TE devices.

Graphyne, a layered carbon allotrope with both sp and sp^2 hybridized bonds, is considered as a possible competitor of graphene for their unique electronic [160], mechanical [161], and adsorption [162] properties. Among the many forms of graphyne, β-graphyne (Figure 10(b)), γ-graphyne (Figure 10(c)), and their nanostructures have been reported to have good TE properties theoretically. For instance, Ouyang et al., using NEGF simulations, revealed that graphyne

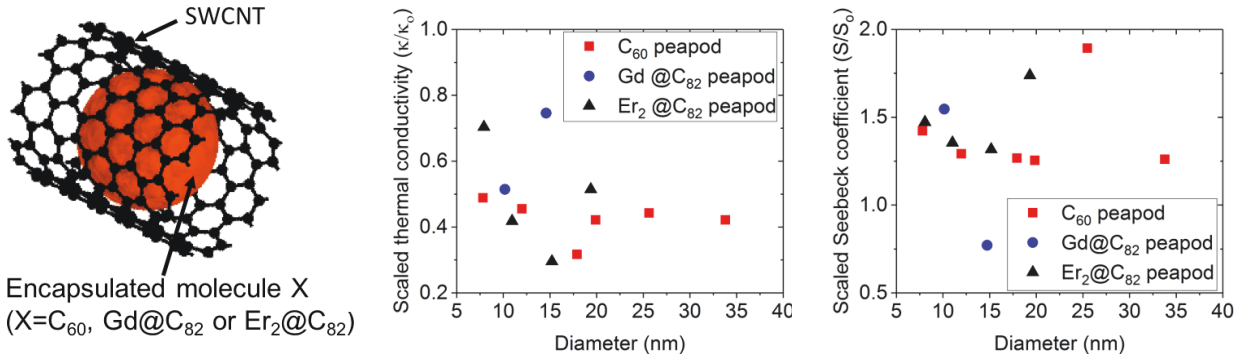

(a) (b) (c)

FIGURE 9: (a) Schematic of SWCNT encapsulated with molecules. ((b) and (c)) Scaled thermal conductivity and Seebeck coefficient as a function of the diameter of CNT [150].

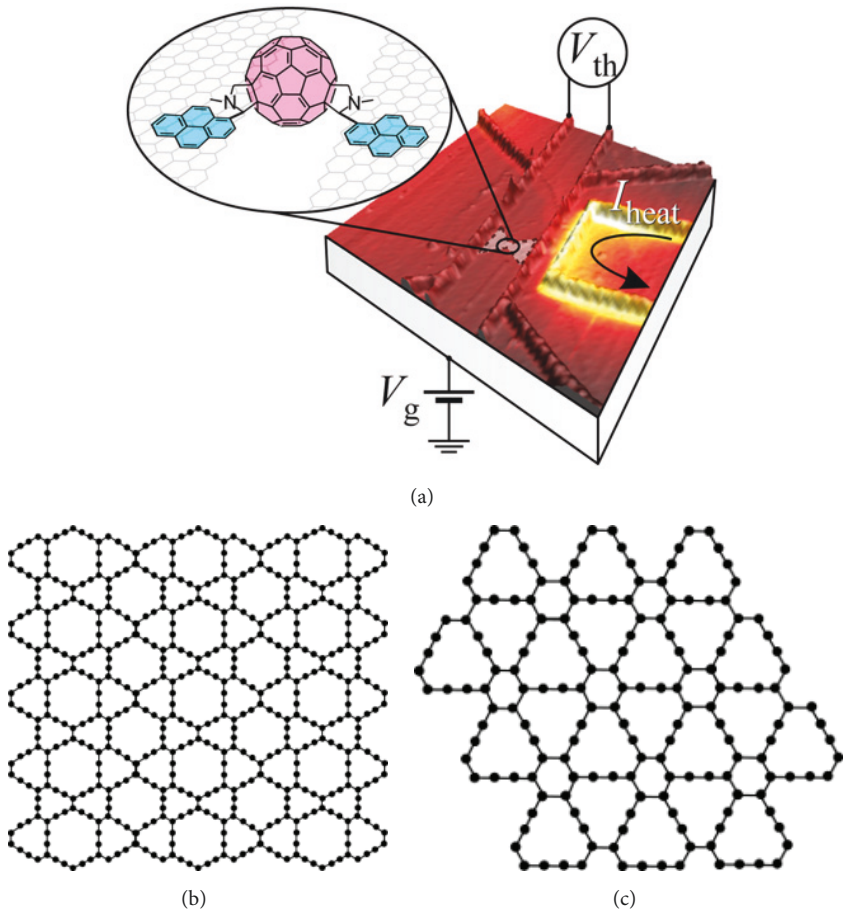

(a)

(b) (c)

FIGURE 10: (a) Schematic of the graphene-fullerene junction TE device fabricated by Gehring et al. ((b) and (c)) Atomic structures of β-graphyne (b) and γ-graphyne. Panel (a) is reproduced with permission [159].

nanoribbons (GyNR) possess better TE properties than the corresponding GNRs with a 3- to 13-fold increase in ZT [163]. They also found that the nanojunction between two GyNRs exhibit better ZT than GyNR, primarily owing to the decreased thermal conductance. Similarly, Zhou et al. investigated the TE properties of β-graphyne and defective (vacancies) β-GyNRs using NEGF simulations [164]. They found that the lattice thermal conductance is reduced substantially by the strong phonon-defect scatterings and phonon localization in defective GyNRs, while the power factor is less deteriorated compared to thermal conductance. As a result, defective β-GyNRs exhibit a higher ZT of 1.64,

around 6 times higher than the corresponding perfect β-GyNR. The above studies indicate the feasibility of the aforementioned "phonon-glass, electron-crystal" concept for these carbon allotropes, and effective reduction of κ_L is crucial for achieving excellent TE performance.

3.6. Carbon Quantum Dots. As revealed by Hicks and Dresselhaus, low-dimensional structures could carry much higher ZT than 3D forms of the same material [26, 27]. Quantum dots (QD), which can be viewed as quasi-0D structures, can have sharp δ-function-like peaks in their density of states, owing to the even stronger quantum confinement in these maximally confined structures. These sharp peaks were predicted to be the optimal electronic structure for TE performance, especially enhanced S, by Mahan and Sofo [165]. Moreover, the strong boundary scattering in QDs can also reduce κ_L substantially to even below that of alloys. In fact, excellent TE properties have been found or predicted for QDs of various materials [28, 29], including carbon QDs [166, 167].

Yan et al. used the atomistic NEGF method to show that hexagonal graphene quantum dots, which can be viewed as a tiny piece of GNR constricted on both sides, can exhibit a ZT higher than that of pristine GNR [166]. In particular, zGNR and aGNR quantum dots can exhibit a maximum ZT of 1.4 and 0.8, respectively, which are much higher than their pristine counterparts. It was also found that the applied constrictions suppress the transmission of high-frequency phonons and, as a result, the lattice thermal conductivity κ_L decreases significantly and thus the ZT increases.

Similar to C_{60}-molecules, the Fermi level of QDs is much easier to control by an external electrical field than the corresponding bulk material. Liu et al. explored the TE properties of an all-carbon quantum device consisting of a graphene QD electrode and two zGNR electrodes using the NEGF method [167]. Specifically, the QD electrode is a zigzag-edged trigonal graphene, which was known to be ferromagnetic at ground state. As the band structures for spin-up and spin-down are different in this ferromagnetic structure, it was shown to have spin-dependent TE properties, including the electrical conductivity and Seebeck coefficient. Interestingly, it was found that the gate voltage, which tunes the Fermi level of the QD, can convert the spin-up component between n-type (negative S) and p-type (positive S), while the spin-down component is rather insensitive to the gate voltage. This work demonstrated the possible feasibility of controlling the TE property of QDs.

3.7. Junction and Network of Carbon Allotropes. If we neglect the coherence of phonons in the GNM structure discussed in Section 3.2, GNM can be viewed as a structure containing periodically arranged graphene nanoconstrictions. Cao et al. [168] studied such nanoconstriction structure using MD simulations and developed a generalized 2D thermal transport model to predict the effective thermal conductivity of networked (series or parallel) nanoconstrictions. The 2D thermal transport model is given as

$$\frac{1}{\kappa} = \frac{1}{\kappa_o} + \frac{l_y \delta}{l_x} \sum_{j-1}^{M} \frac{\pi}{2\delta v_g c_v \sum_{i-1}^{N_j} W_i}, \quad (16)$$

where l_x and l_y are the system length and width, respectively, k_o is the thermal conductivity of pristine graphene, v_g is the phonon group velocity, c_v is the volumetric heat capacity, W_i is the width of the i-th constriction, and M and N are the number of constriction in series and in parallel, respectively. Based on this model, it is obvious that narrower constrictions lead to lower thermal conductivity. The reduction in thermal conductivity is attributed to the strong phonon localization at the edges of the nanoconstrictions, as has been revealed in [55, 56, 169], and the change in phonon transmission angle. The tunable and ultralow κ_L obtained in Cao et al. work suggests the potential use of graphene nanoconstriction networks for thermoelectrics.

Unlike the above kinked GNR and graphene nanoconstriction structures, in which GNRs are connected in the basal plane, Nguyen et al. used a tight-binding-based NEGF method to investigate the TE properties of a bilayer vertical graphene junction structure [170]. They found that the weak interlayer van der Waals interactions can reduce κ_L of the bilayer graphene structure, while electron transport is much less affected. Moreover, by making the bilayer graphene a bilayer GNM, a high ZT~1 can be obtained, which suggests the possibility that bandgap engineering and phononic engineering, if synergistically combined, can be used to realize high ZT graphene-based TE materials.

In addition to the single materials or homojunctions discussed above, combining different carbon allotropes into one heterojunction has also been investigated as a route towards better TE materials. Zhou et al., using first-principles-based NEGF simulations, investigated the TE properties of heterojunctions between aGNRs and armchair GyNRs and found that phonon transport is substantially suppressed at the GNR-GyNR interfaces [171]. Moreover, S can be enhanced by the interference between electron waves scattered at the interfaces. Consequently, the maximum ZT of the GNR-GyNR heterojunctions could be 5 to 14 times higher than that of pristine aGNRs. The authors also found that the ZT of such heterojunctions can be readily tuned by choosing different edge chirality and types of GyNR, which indicates the possible usefulness of these structures for thermoelectrics.

4. Carbon Materials Based Composites

In the past decades, a significant amount of efforts have been devoted to developing polymer-based TE materials due to their relatively lower cost for manufacturing, light weight, mechanical flexibility, and environmentally benign characteristics [38–40]. The inherently low thermal conductivity (typically < 1 W/m-K) of polymers is beneficial for TE applications. However, most of the polymers have very low electrical conductivity and Seebeck coefficient, which require doping or combining with other materials into a composite to achieve better TE performance. Since increasing σ and S is almost always more important than reducing κ_L for improving the TE performance of polymers or polymer-based composites, publications in this area usually only report the power factor rather than ZT. On the other hand, some types of modified CNTs or graphene can exhibit good electrical performance, but their high κ_L

renders them impractical for TE applications. Other than engineering the structure of carbon allotropes as discussed in the previous sections, synthesizing composites by combining carbon allotropes with polymers appears to be a potential solution to this problem [172]. In general, the composites formed in this way could possess electrical conductivities close to films exclusively composed of CNTs, because the charge carriers can travel through the nanotube network by hopping. At the same time, the major heat carriers, phonons, are strongly scattered at the surfaces of CNTs, the junctions between the tubes, and the interfaces between CNT and polymers. Therefore, CNT-based composites could possess high electrical conductivity and low thermal conductivity.

Though not as popular as polymer-based composites, there have also been attempts to fabricate composites composed of CNT and ceramic TE materials [173–175]. Besides, chemically bonding CNT or graphene with other materials into a metamaterial [176–178], which can be viewed as a simple composite, was also investigated as a route towards future TE applications, which will be discussed at the end of this section.

4.1. Carbon Material-Polymer Composites. Polymer-based TE materials are being actively investigated as a route towards flexible, printable, and cheap TE materials. Figure 11 summarizes notable data regarding S and σ of TE composites composed of CNT/graphene and polymers [179–203]. As we can see, both intrinsically insulating polymers and conductive conjugated polymers have been explored extensively, demonstrating promising values of S up to ~140 μV/K and σ approaching 10,000 S/cm. However, there are also great challenges associated with CNT/graphene-polymer composites. For example, the air stability of n-type polymer-based composites has imposed great barrier for the development of practical n-type organic TE materials. This issue is also reflected in Figure 11, which shows the more diverse data for p-type composites than n-type ones. Besides, it is also important and challenging to form continuous CNT/graphene networks for efficient charge transfer and ensure that the CNT/graphene fillers are well dispersed in the polymer matrix. All of these issues will be discussed in this subsection.

In 2006, Yu et al. [204] fabricated CNT-poly(vinyl acetate)(PVAc) composites with a maximum room-temperature ZT of 0.006, which was a more than 6-fold improvement over the state-of-the-art polymer-based composites at that time. In their work, a mixture of metallic and semiconducting single-, double-, and triple-walled CNTs was suspended in a PVAc emulsion to make a composite, of which the schematic and SEM image are shown in Figures 12(a) and 12(b), respectively. As we can see, the resulting composite has a rather uniform network of CNTs, which wrap around the PVAc emulsion particles. Since phonons experience substantial scatterings at the CNT-CNT junctions, the overall thermal conductivity is very low (0.25-0.40 W/m-K in Figure 12(c)). PVAc, in spite of being an insulating polymer, manifests a monotonic increment of electrical conductivity as the concentration of incorporated (in a network fashion) CNT increases (Figure 12(d)). This is because electrons can be efficiently transmitted by hopping between CNTs. As displayed in Figure 12(d), the thermopower (Seebeck coefficient) was not affected much by the concentration of CNT. The net effect of increasing CNT concentration is thus an increase in ZT.

To make the above CNT-PVAc composites, stabilizers must be used to prevent CNTs from complete dispersion or exfoliation in water. Recognizing the possibly strong influence of stabilizers on electron transport across CNT-CNT junctions [205], which determines the overall TE performance of the composite, Moriarty et al. compared the TE properties of DWCNT-PVAc and MWCNT-PVAc composites with two different stabilizers: the insulating sodium deoxycholate (DOC) and semiconductive meso-tetra(4-carboxyphenyl) porphine (TCPP) [206]. They found that S of MWCNT-based composites containing 12 wt% CNT increased from 7.9 μV/K to 28.1 μV/K when the stabilizer was switched from DOC to TCPP, which was attributed to either a lower carrier concentration or a larger effective mass of the carriers in TCPP than DOC. For DWCNT-based composites containing 12 wt% CNT, replacing DOC with TCPP can cause a substantial increase in σ from 1,474 S/m to 7,108 S/m. This is because the insulating DOC stabilizer hinders tube-to-tube electron transfer.

In addition to PVAc, other intrinsically insulating polymers like Nafion [179] were also investigated for TE properties. However, a significant drawback of insulating-polymer-based composites is the intrinsically low electrical conductivity. As shown in Figure 11, the data points for PVAc and Nafion-based composites are located at the low-σ region of the graph. The low σ thus seriously limits the power factor of insulating-polymer-based composites. Therefore, there have been attempts to develop intrinsically conductive-polymer-based ones, among which conjugated polymers have received the most attention, as discussed below.

In 2010, Kim et al. [205] fabricated composites composed of CNT and poly (3,4-ethylenedioxythiophene): poly(styrenesulfonate)(PEDOT:PSS), a well-studied conjugated polymer. This composite was found to have a high σ up to 40,000 S/m, owing to the intrinsic electrical conductivity of PEDOT:PSS and the unique junction between CNT and PEDOT:PSS that enables efficient transfer of charges through the CNT network. The Seebeck coefficient S was almost unaltered by the addition of PEDOT:PSS, because the small energy barrier for electron transport at the junctions hinders the transport of low-energy charges, making S insensitive to the increase in electrical conductivity. Moreover, as we can see in Figure 12(e), σ increases almost proportionally with the weight fraction of CNT (mixture of metallic and semiconductive single-, double-, and triple-walled CNTs), while the thermal conductivity increases much less and remains low, owing to the distinctly different lattice properties of CNT and PEDOT:PSS. As a result of the decoupled TE properties, a ZT of up to 0.02 was achieved in CNT-PEDOT:PSS composite containing high-purity SWCNTs, which is at least one order of magnitude higher than the ZT of most polymers reported previously.

In 2012, another group reported that graphene is more effective in improving the TE properties of PEDOT:PSS compared to CNT [207]. Specifically, 30-40 wt% (weight percent) CNT is required to enhance the TE property of

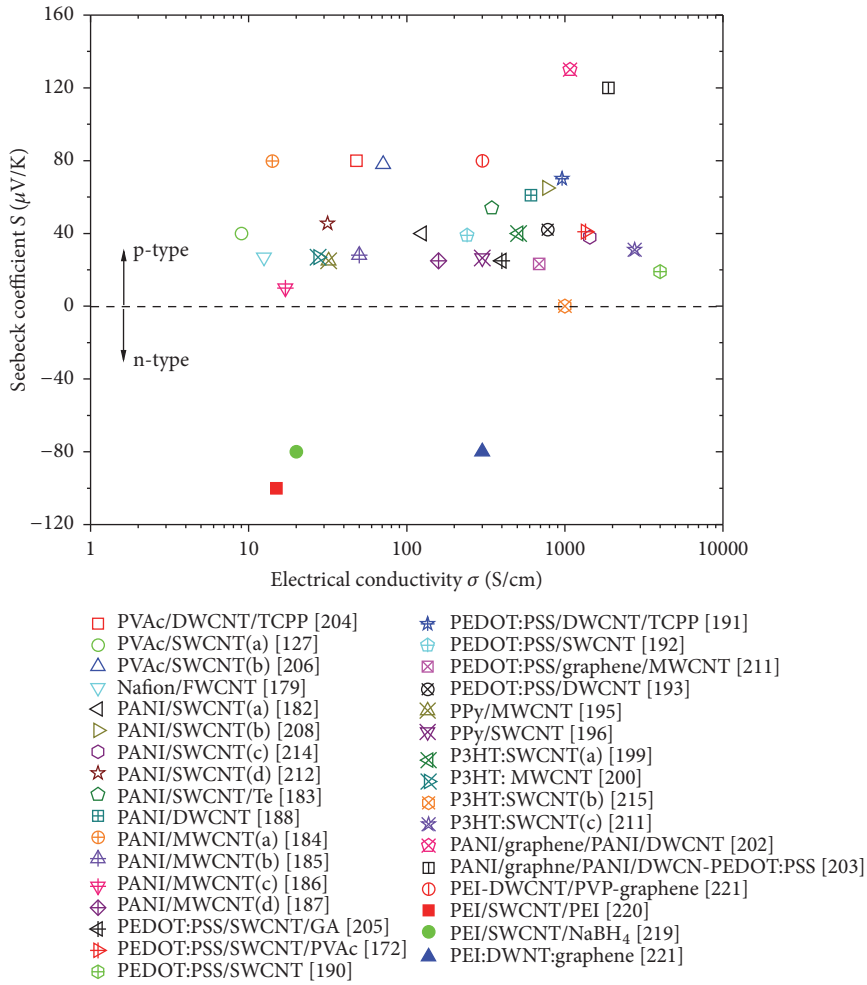

Figure 11: Seebeck coefficient and electrical conductivity of composites of CNT or graphene with polymers measured in previous studies.

PEDOT:PSS, while only 2 wt% graphene can increase the ZT of PEDOT:PSS by 10 times. Strong π-π bonding that facilitates the dispersion was observed in graphene-embedded PEDOT:PSS thin films. Besides, the enhanced contact area of graphene-PEDOT:PSS, which is 2-10 times higher than CNT-PEDOT:PSS composite with the same weight percentage, also facilitates carrier transfer between PEDOT:PSS and graphene. Higher carrier mobility and lower thermal conductivity caused by the porous structure of PEDOT:PSS thin films containing 2 wt% graphene can lead to a ZT of 0.02, which is comparable or even higher than those containing 35 wt% CNTs [204, 205].

In addition to PEDOS:PSS, other types of conjugated polymers, such as polyaniline (PANI), poly 3-hexylthiophene (P3HT), and polypyrrole (PPy), have also been studied extensively for TE applications. For instance, PANI has received extensive research attention for the straightforward preparation protocol, excellent tunability of electrical properties, and low manufacturing cost [208].

In 2009, Gui et al. fabricated sponge-like 3D CNT networks (Figure 13(a)) with an extremely low thermal conductivity of 0.035 W/m-K [209]. Based on this structure, Chen et al. synthesized a flexible CNT-PANI composite (Figure 13(b)) with significantly improved TE performance compared to pure PANI [210]. The CNT-PANI network demonstrated significant improvement in terms of electrical conductivity (Figure 13(c)) and thermopower, or Seebeck coefficient (Figure 13(d)) compared to pure PANI. However, the power factor was still low, with the best being 2.2 μW/m-K^2. Another advantage of the CNT-PANI network is that it retained the structural flexibility of the 3D CNT network, as displayed in the inset of Figure 13(b).

Yao et al., in 2010, observed a maximum power factor of 20 μW/m-K^2 in SWCNT-PANI composites [182], which is over 2 orders of magnitude higher than that of pure PANI (~ 0.01 μW/m-K^2). In their work, the composites were prepared by in situ polymerization reaction, in which the CNTs acted as templates and the PANI reactants grew on the surface of CNTs. It was found that the PANIs generated with this process possess more aligned molecular structure, which may result from the strong π-π interactions between CNT and PANI. As a result of the enhanced structural regularity, the electrical conductivity and Seebeck coefficient were greatly improved compared to pure PANI, while the thermal conductivity

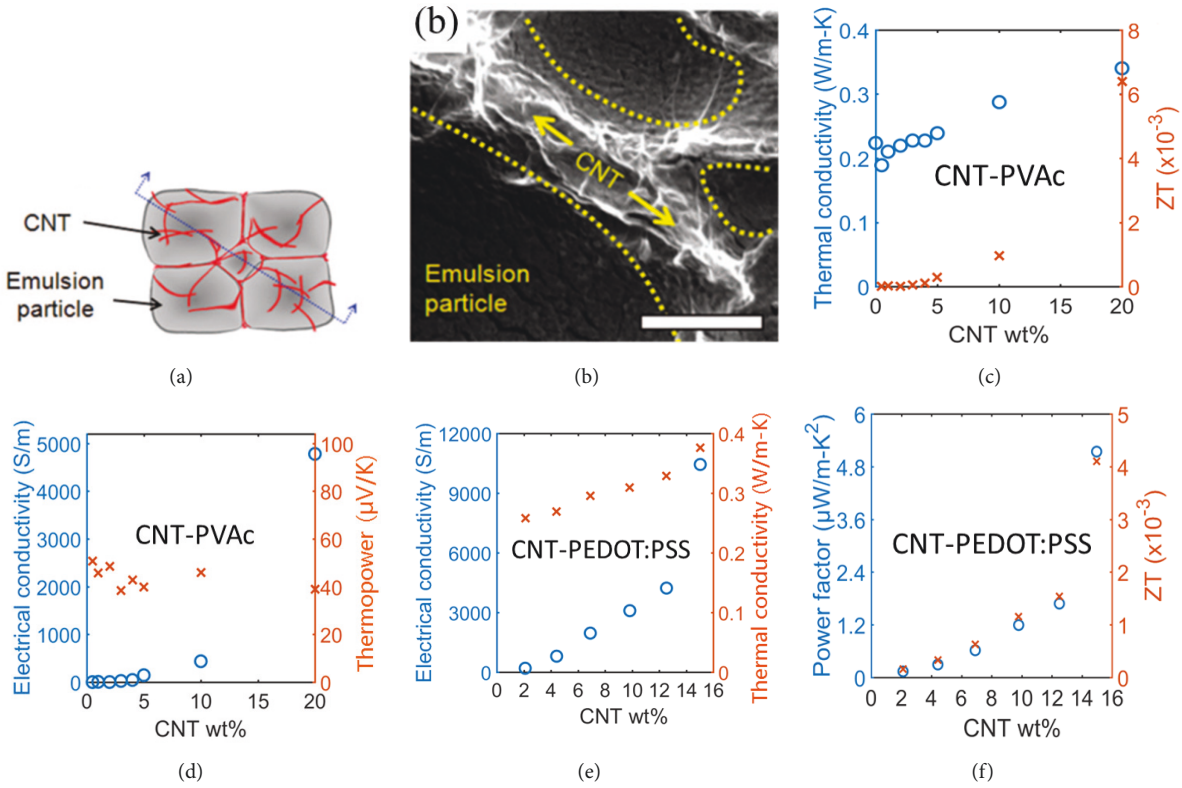

FIGURE 12: ((a) and (b)) The schematic and SEM image of the CNT-PVAc composite [204]. (c)–(f) Thermal conductivity, ZT, electrical conductivity, and thermopower (Seebeck coefficient) of the CNT-PVAc or CNT-PEDOT:PSS composites as a function of the weight percent of CNT [204, 205]. Panels (a) and (b) are reproduced with permission [204].

remained low due to the intense phonon scatterings at the SWCNT/PANI interface. Similarly, Liu et al. produced paper-like SWCNT-PANI composite files using an electrochemical polymerization technique [212]. In their work, the strong π-π interaction between CNT and PANI was believed to cause a shift in carrier density and Fermi level, leading to increased carrier density and Seebeck coefficient. The best power factor of the SWCNT-PANI composite produced in Liu et al. work is 6.5 μW/m-K^2 [212].

The strong π-π interaction between CNT and conjugated polymers like PANI is not always beneficial for fabricating composites of these materials. In fact, it renders it challenging to obtain well-dispersed composites. Yan et al. adopted a two-step approach to overcome this problem: first, they premixed PANI and CNT using in situ polymerization; then they hot-pressed the mixture into a PANI matrix to obtain the composite [213]. In this manner, PANI was well coated onto the surface of CNT. However, the maximum power factor measured for such composites was only ~1.5 μW/m-K^2, much lower than the 20 μW/m-K^2 obtained in Yao et al.'s work discussed earlier [182], which primarily arises from the significantly lower σ. Less contact between CNTs might be the cause of the reduced σ, which suggests the importance of maintaining a balance between the degree of dispersion of CNTs in the composites (for structural homogeneity) and the amount of contacts between CNTs (for higher σ of the CNT network).

In 2014, Yao et al. synthesized SWCNT-PANI composites with an even higher power factor of 176 μW/m-K^2 [208], by dissolving camphor sulfonic acid (CSA)-doped PANI in m-cresol solvent to expand the PANI coil. As shown in Figure 14, the expanded PANI had larger area to interact with SWCNTs, leading to more ordered composite structure. In 2016, the same research group reported a further increased power factor of 217 μW/m-K^2 for SWCNT-PANI composites produced from the similar process [214]. In both studies [208, 214], the substantially enhanced power factor compared to earlier studies [182, 212, 213] is primarily caused by the orders of magnitude improvement in σ, which is enabled by the much better structural regularity.

Bounioux et al. demonstrated encouraging TE performance in CNT-P3HT composite films, in which the conjugated polymer P3HT is sufficiently p-doped along with the CNT [215]. Since the p-doped polymer matrix facilitates carrier transport alongside CNT, the overall electrical conductivity and hence the power factor of the composite were increased. In particular, the authors found that optimally doped samples containing 8 wt% SWCNTs exhibited an electrical conductivity of 1,000 S/cm and a power factor of 95 ± 12 μW/m-K^2.

Hong et al. achieved even better TE performance (power factor of 267 ± 38 μW/m-K^2) in SWCNT-P3HT hybrid films, in which P3HT was doped by spin-coating [211]. In contrast, the films doped with the conventional immersion method,

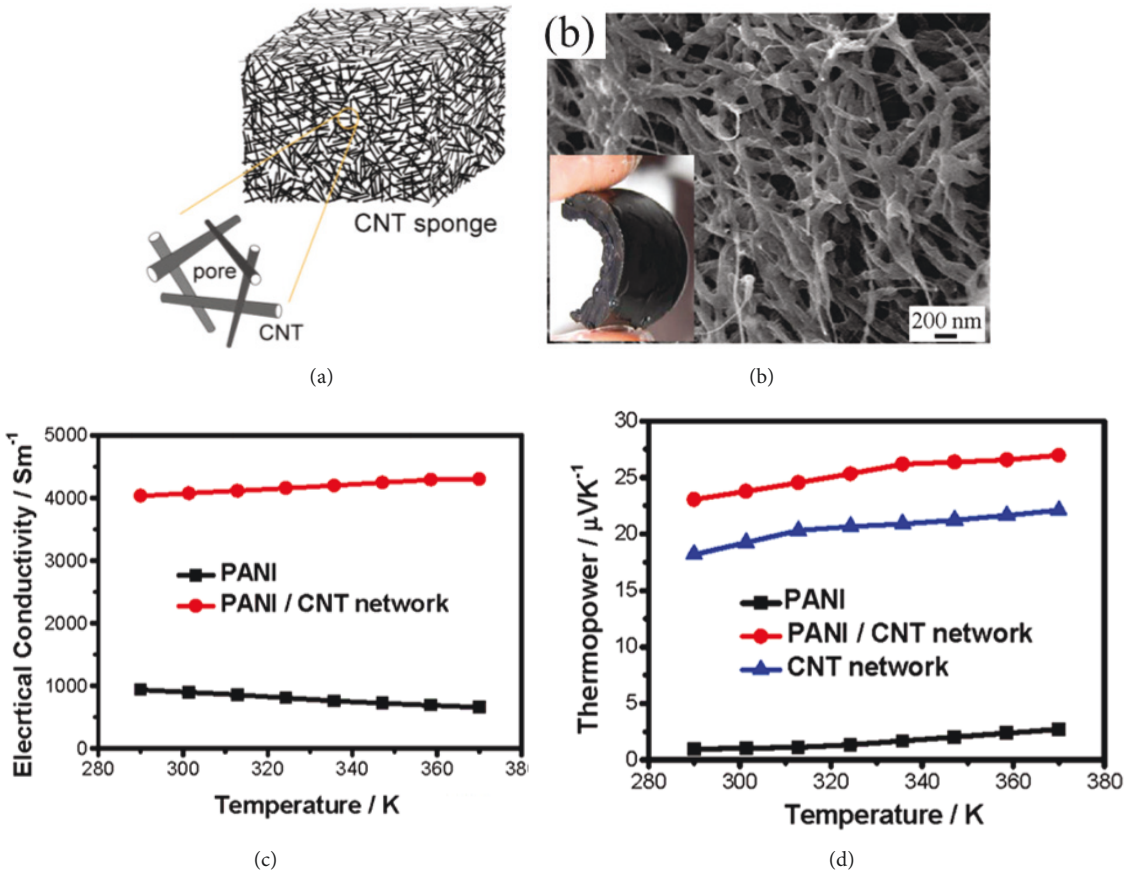

FIGURE 13: (a) Schematic of the CNT sponge [209] (b) SEM image of the CNT-PANI composite. The inset shows its macrophoto. ((c) and (d)) Electrical conductivity and thermopower of pure PANI, CNT-PANI composite, and pure CNT network as a function of temperature [210]. All panels are reproduced with permission [209, 210].

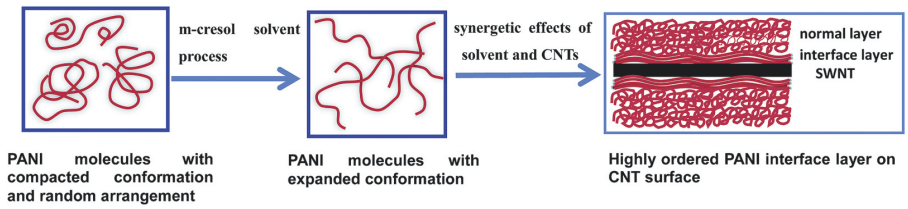

FIGURE 14: Schematics showing the process for forming ordered PANI interface layer by the synergistic effects of the solvent process and the π–π conjugation between PANI and CNTs. Figure is reproduced with permission [208].

which was also used in an earlier study [215], only demonstrated a power factor of 103 ± 24 μW/m-K^2. The reason lies in the fact that spin-coating can dope the P3HT matrix more efficiently and thus leads to higher σ, as shown in Figure 15. Subsequently, the same research group observed even higher power factor (325 ± 101 μW/m-K^2) in CNT-P3HT composites containing few-walled CNTs (2-4 walls), which was attributed to the higher σ in DWCNTs than SWCNTs [216].

It is worth mentioning that all the composites discussed above are p-type, i.e., possessing a positive S. In practical TE devices, it is usually beneficial to alternately connect p-type and n-type TE components in series to achieve larger power generation. Unfortunately, n-type organic materials are usually unstable in air and/or electrically resistive, which imposes a great challenge to realize polymer-based TE devices. Among the many methods used, n-type doping of CNT using reducing agents like hydrazine [217, 218], sodium borohydride ($NaBH_4$), polyethyleneimine (PEI) [219] has been mostly studied. For instance, Yu et al. doped chemical vapor deposition (CVD)-grown CNTs with PEI and $NaBH_4$ [219]. They have achieved promising n-type TE properties with a large S of -80 μV/K. In contrast, if CNTs are only doped with $NaBH_4$ or PEI, S of the resulting composite is only -24 μV/K and -57 μV/K, respectively.

Freeman et al. [220] fabricated n-type CNT-filled polymer composites by first dispersing CNTs with sodium

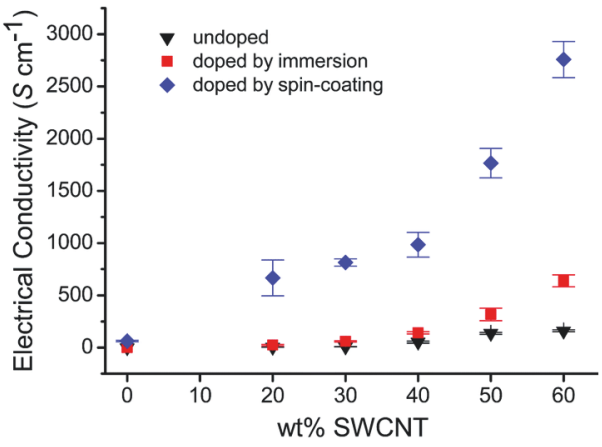

FIGURE 15: Electrical conductivity of the SWCNT-P3HT hybrid films, in which the P3HT matrix was undoped, doped by immersion, and doped by spin-coating, as a function of the mass fraction of SWCNT. Figure is reproduced with permission [211].

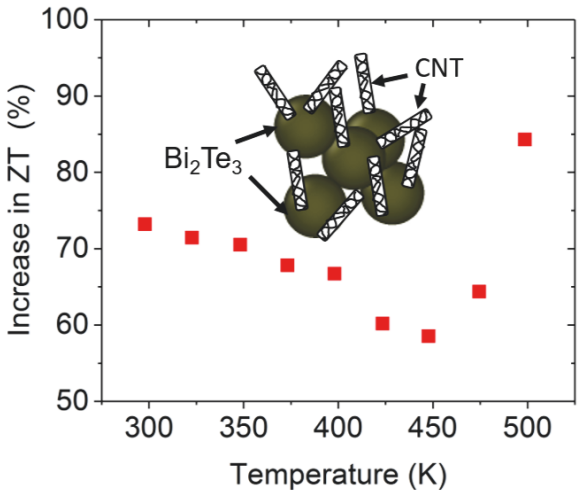

FIGURE 16: Increase in the ZT of Bi_2Te_3 by creating MWCNT-Bi_2Te_3 composite [173]. The inset shows the schematic of the composite.

dodecylbenzenesulfonate (SDBS), then functionalizing them with PEI, and finally making them into composites with PVAc. The resulting composite was air-stable and displayed good σ around 1,500 S/m, S around -100 μV/K, and thus a power factor around 15 μW/m-K^2. Moreover, it was found that higher SDBS surfactant percentage caused smoother cleavage, fewer CNT pullout, and less CNT agglomeration, which are the characteristics of good dispersion. As a result, the high σ of CNT was not much deteriorated. Even though σ and S are usually inversely related to each other, the authors found that both properties were improved in samples with a higher SDBS percentage, which was attributed to the enlarged sites for PEI doping resulting from the better CNT dispersion.

Cho et al., using a layer-by-layer (LBL) assembly technique, fabricated a stable n-type TE multilayer thin film by alternately depositing DWCNT and graphene, which were stabilized by PEI and polyvinylpyrrolidone (PVP), respectively [221]. The resulting thin film exhibited a high power factor of 190 μW/m-K^2. Different from conventional bulk TE materials, both σ and S of the PEI:DWCNT:PVP:graphene films increased as the number of deposited bilayers increased. The decoupling of σ and S was attributed to the fact that the resulting 3D network, working as a low-energy electron filter, preferentially allows the transfer of high-energy charges, which increases S. Moreover, S is relatively air-stable over 60 days with no protection, which stems from the fact that the film obtained by such LBL deposition technique consists of highly aligned and exfoliated granular graphene layers with extreme tortuosity, i.e., high resistance to gas diffusion or oxygen permeability.

Unlike typical inorganic TE materials, CNT-polymer composites are mostly thin films [222], of which the small thickness limits the maximum temperature difference attainable in the perpendicular direction of the film surface and thus limits the maximum output voltage. To solve this problem, Hewitt et al. [223] proposed a felt-fabric-like multilayered TE module, where temperature gradient parallel to the module surface is applied. Specifically, the authors arranged the p-type and n-type PVDF-MWCNT films one over another alternately, between which an undoped PVDF film is sandwiched to avoid short circuit. The resulting felt-fabric-like TE module works as if multiple voltage sources are connected in series. In Hewitt et al.'s work, the TE module consisting of 72 layers of PVDF-MWCNT (95 wt%) films demonstrated a Seebeck coefficient of 550 μV/K and output voltage of 51 mV, when the temperature bias was 95 K.

Recently, Olaya et al. found a high ZT for layered graphene-based TE devices at room temperature [224]. The device is composed of electrochemically exfoliated graphene layers separated by phonon-blocking materials such as PEDOT:PSS, PANI, and gold nanoparticles. Remarkably high values of ZT in the range of 0.81-2.45 were measured. In particular, the room-temperature ZT of ~2 for graphene-PEDOT:PSS is even comparable to the best inorganic TE materials studied so far.

4.2. Carbon Material-Inorganic Material Composites. Unlike the CNT/graphene-polymer composites discussed in the previous section, there are much fewer studies [174, 175] on CNT-ceramic TE materials because of the challenge of dispersing CNTs homogeneously in a ceramic matrix [173]. Kim et al. approached this problem through a chemical way based on a molecular-level mixing process, in which MWCNTs were homogeneously embedded into Bi_2Te_3 powders [173]. The resulting MWCNT-Bi_2Te_3 composite, of which the schematic is shown in Figure 16, exhibited a 55%-90% increase in ZT compared to pure Bi_2Te_3 in the temperature range of 298-498 K. Specifically, the room-temperature ZT is increased from 0.28 to 0.48. The addition of CNTs was found to reduce the carrier concentration and, consequently, the Seebeck coefficient was increased. Specifically, the MWCNT-Bi_2Te_3 composites exhibited an S of -113 μV/K, much higher than the S = -83 μV/K of pure Bi_2Te_3. Moreover, the composite exhibited a low thermal conductivity of 0.65 W/m-K, about

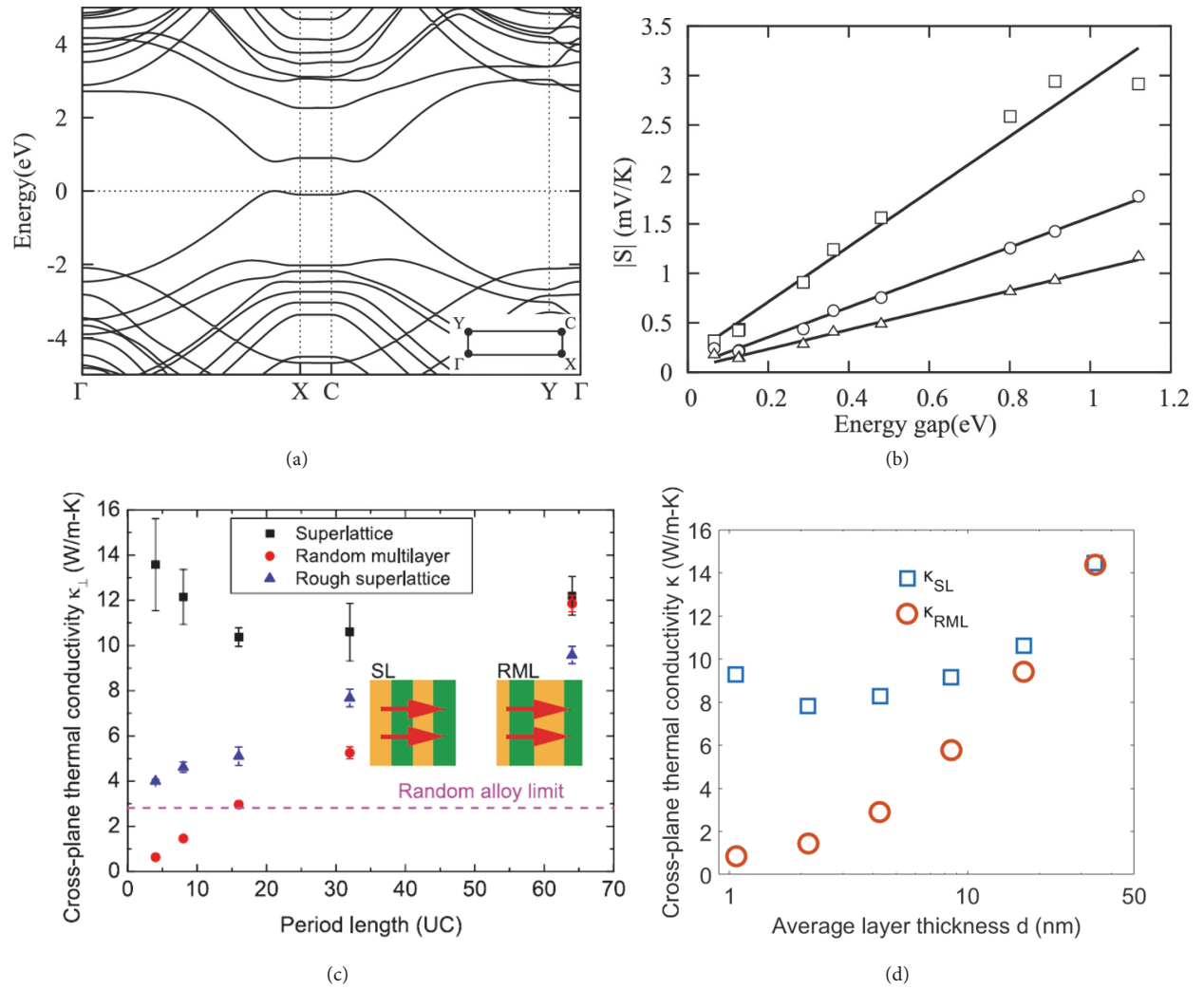

FIGURE 17: (a) Band structure of a zGNR/zBNNR superlattice consisting of 2 dimer lines of zGNR and 6 dimer lines of zBNNR [176]. (b) Seebeck coefficient as a function of bandgaps for the zGNR/zBNNR superlattices [176]. Squares, circles, and triangles are for 150 K, 300 K, and 450 K, respectively. (c) Cross-plane thermal conductivity of superlattice, random multilayer, rough superlattice, and random alloy for a Lennard-Jones type conceptual crystal [33]. (d) Thermal conductivity of conceptual Lennard-Jones superlattices and random multilayers as a function of average layer thickness [34]. Panels (a)–(c) are reproduced with permission [33, 176].

40% lower than that of Bi_2Te_3. As a result, a significant enhancement in ZT was achieved, as shown in Figure 16. The MWCNT-Bi_2Te_3 interfaces were believed to cause the reduction in thermal conductivity by scattering phonons strongly. The MWCNT-Bi_2Te_3 composite showed a very encouraging maximum ZT of 0.85 at 473 K. This work paved the way for fabricating TE composites based on CNT and ceramic TE materials.

In addition to the above work on MWCNT-Bi_2Te_3, there are also successful attempts in combining other well-known outstanding TE materials, e.g., PbTe and SnSe, with graphene or CNTs into composites [225–228]. Typically, phonons in PbTe and SnSe are already strongly scattered, while the addition of carbon nanomaterials sometimes can cause a further reduction in κ_L owing to the increased amount of heterogeneous grain boundaries. More importantly, CNT and graphene can serve as electron transport channels to greatly enhance electrical conductivity, which usually leads to significant increased power factor.

Yokomizo et al. [176] have theoretically shown that a superlattice consisting of zGNRs and zigzag hexagonal boron nitride (h-BN) nanoribbons (zBNNRs) can attain about 20 times larger Seebeck coefficient than that in single crystalline graphene. zGNRs are typically known to be metallic, which renders them not suitable as TE materials. However, it has been reported that a static external electric field could cause bandgap opening in zGNRs [229]. Inspired by this finding, Yokomizo et al. hypothesized that an internal electric field can be induced at the zGNR/zBNNR interface due to the polar nature of zBNNR, which would open a bandgap in the zGNR/BNNR superlattice. Moreover, the zGNR/zBNNR superlattice exhibits a pudding-mold-type band (Figure 17(a)), of which the top is flat but bends steeply into a dispersive band [230]. This peculiar band structure endows

the zGNR/zBNNR superlattice with a much higher room-temperature Seebeck coefficient (1,780 μV/K at maximum) than single zGNR (282 μV/K), as shown in Figure 17(b). In fact, thermal transport in similar superlattices has been investigated computationally and a significant reduction in κ_L compared to pure GNR or graphene has been observed [231–234].

Shiomi et al. [177] conducted nonequilibrium MD simulations to study the feasibility of isotopically modifying SWCNT into a superlattice to achieve ultralow κ_L. The superlattice was constructed by alternately connecting ^{12}C and ^{13}C (or ^{24}C) SWCNTs. κ_L of $^{12}C/^{13}C$ ($^{12}C/^{24}C$) SWCNT superlattices can be attenuated to as low as 56%(5%) of that of ^{12}C SWCNT. κ_L reaches the minimum value at a critical period thickness due to the crossover of zone-folding effect and the thermal boundary resistance effect, which was well understood for other types of superlattices [95]. The resulting low κ_L, however, still cannot beat the random alloy limit.

Regarding the inability to beat the random alloy limit in isotopically modified SWCNT superlattice, there indeed exists a new strategy by creating random multilayer structures to block the coherent phonons that contribute a significant amount of heat transfer in regular superlattices [33, 34, 57, 235]. As shown in Figures 17(c) and 17(d), κ_L of superlattice can be reduced substantially by randomizing its layer thickness, which then becomes a random multilayer. A prominent study on $^{12}C/^{13}C$ graphene superlattice was conducted by Mu et al. [178], in which MD simulations were performed to investigate coherent and incoherent phonon transport as affected by the periodicity of the structure. One interest finding made by Mu et al. is that κ_L of the carbon superlattice can be reduced substantially by randomizing the thicknesses of ^{12}C and ^{13}C layers, which was attributed to the localization of coherent phonons. The tunable and ultralow lattice thermal conductivity makes $^{12}C/^{13}C$ heterostructure promising for TE applications.

5. Conclusion and Outlook

In this review, we have discussed recent advances in TE materials based on carbon allotropes, including CNT, graphene, fullerene, graphyne, and TE composites combining the above carbon allotropes with other organic or inorganic materials. Evidently, the common carbon allotropes are not suitable as TE materials in their raw forms, because of their high thermal conductivity, low Seebeck coefficient, or low electrical conductivity. However, we have demonstrated through a review of recent literature that it is possible to modify their thermal and electrical properties substantially by introducing defects, applying strain, controlling structural topology, creating phononic crystals, or combining with other materials into composites. In particular, these strategies can at least improve the TE properties of the original carbon-based materials in one of the following aspects: reducing the lattice thermal conductivity without decreasing the electrical conductivity by the same amount; increasing the electrical conductivity; or increasing the Seebeck coefficient. It is also worth noting that even though theoretical studies have predicted very high ZT for some of the materials discussed in this review, it generally demands sophisticated fabrication techniques to precisely engineer the structures and materials in the designed forms, which is either unrealistic with currently available technology or too costly for mass production. In that sense, composites combining the strengths of carbon-based materials with other materials, particularly polymers, provide a cost-effective and scalable way to enable the wide application of TE materials. It has also been demonstrated that polymer-based composites can possibly achieve better mechanical properties than inorganic TE materials, which tend to be brittle owing to the lack of metallic bonds in TE materials that are mostly semiconductors. Nonetheless, as we can see from this review, the power factor and ZT of carbon materials-polymer composites are still far from being ideal. The major challenge lies in the low electrical conductivity and unsatisfactory Seebeck coefficient. Therefore, extensive research efforts are still needed for developing chemical and material processing strategies to fabricate effectively doped materials or air-stable n-type organic-inorganic composites and discovering conductive polymers with better TE properties. Currently, DFT-based first-principles predictive simulations are usually limited to supercells of a few hundreds of atoms. Even though classical MD simulations have enabled researchers to study much larger systems (millions of atoms), the need for interatomic potentials, the lack of accuracy (especially for thermal transport) in existing potentials, and the inability in naturally modeling electron-phonon coupled thermal transport [236] have imposed great challenges for a wider application of this method. Therefore, the advancement in materials modeling and simulation would benefit the development of novel high-performance TE materials profoundly.

Conflicts of Interest

The authors declare that there are no conflicts of interest regarding the publication of this article.

Funding

Pranay Chakraborty, Tengfei Ma, and Yan Wang have been supported by the faculty startup fund from the University of Nevada, Reno. Amir Hassan Zahiri and Lei Cao have been supported by the National Science Foundation (Grant no. CMMI-1727428) and the faculty startup fund from the University of Nevada, Reno.

References

[1] C. Goupil, *Continuum Theory and Modeling of Thermoelectric Elements*, John Wiley & Sons, 2015.

[2] "LLNL Flow Charts," 2017, https://flowcharts.llnl.gov/.

[3] L.-D. Zhao, S.-H. Lo, Y. Zhang et al., "Ultralow thermal conductivity and high thermoelectric figure of merit in SnSe crystals," *Nature*, vol. 508, no. 7496, pp. 373–377, 2014.

[4] G. A. Slack, *CRC Handbook of Thermoelectrics*, D. M. Rowe, Ed., CRC Press, Boca Raton, FL, USA, 1995.

[5] J. L. Blackburn, A. J. Ferguson, C. Cho, and J. C. Grunlan, "Thermoelectric materials: carbon-nanotube-based thermoelectric materials and devices," *Advanced Materials*, vol. 30, no. 11, p. 1870072, 2018 (English).

[6] J. P. Heremans, V. Jovovic, E. S. Toberer et al., "Enhancement of thermoelectric efficiency in PbTe by distortion of the electronic density of states," *Science*, vol. 321, no. 5888, pp. 554–557, 2008.

[7] O. Delaire, J. Ma, K. Marty et al., "Giant anharmonic phonon scattering in PbTe," *Nature Materials*, vol. 10, no. 8, pp. 614–619, 2011 (English).

[8] S. W. Finefrock, Y. Wang, J. B. Ferguson et al., "Measurement of thermal conductivity of PbTe nanocrystal coated glass fibers by the 3ω method," *Nano Letters*, vol. 13, no. 11, pp. 5006–5012, 2013.

[9] Z. Tian, J. Garg, K. Esfarjani, T. Shiga, J. Shiomi, and G. Chen, " Phonon conduction in PbSe, PbTe, and PbTe ," *Physical Review B: Condensed Matter and Materials Physics*, vol. 85, no. 18, 2012.

[10] B. Xu, M. T. Agne, T. Feng et al., "Nanocomposites from solution-synthesized PbTe-BiSbTe nanoheterostructure with unity figure of merit at low-medium temperatures (500-600 K)," *Advanced Materials*, vol. 29, no. 10, p. 1605140, 2017.

[11] Y. Pei, X. Shi, A. LaLonde, H. Wang, L. Chen, and G. J. Snyder, "Convergence of electronic bands for high performance bulk thermoelectrics," *Nature*, vol. 473, no. 7345, pp. 66–69, 2011.

[12] B. C. Sales, D. Mandrus, and R. K. Williams, "Filled skutterudite antimonides: a new class of thermoelectric materials," *Science*, vol. 272, no. 5266, pp. 1325–1328, 1996.

[13] G. S. Nolas, D. T. Morelli, and T. M. Tritt, "Skutterudites: a phonon-glass-electron crystal approach to advanced thermoelectric energy conversion applications," *Annual Review of Materials Research*, vol. 29, no. 1, pp. 89–116, 1999 (English).

[14] X. Shi, J. Yang, J. R. Salvador et al., "Multiple-filled skutterudites: High thermoelectric figure of merit through separately optimizing electrical and thermal transports," *Journal of the American Chemical Society*, vol. 133, no. 20, pp. 7837–7846, 2011.

[15] G. S. Nolas, J. L. Cohn, G. A. Slack, and S. B. Schujman, "Semiconducting Ge clathrates: promising candidates for thermoelectric applications," *Applied Physics Letters*, vol. 73, no. 2, pp. 178–180, 1998 (English).

[16] H. Liu, X. Shi, F. Xu et al., "Copper ion liquid-like thermoelectrics," *Nature Materials*, vol. 11, no. 5, pp. 422–425, 2012.

[17] Y. Wang, N. S. Rogado, R. J. Cava, and N. P. Ong, "Spin entropy as the likely source of enhanced thermopower in $Na_xCo_2O_4$," *Nature*, vol. 423, no. 6938, pp. 425–428, 2003 (English).

[18] K. Fujita, T. Mochida, and K. Nakamura, "High-temperature thermoelectric properties of NaxCoO2-δ single crystals," in *Proceedings of the 20th International Conference on Thermoelectrics (ICT '01)*, pp. 168–171, June 2001.

[19] K. Koumoto, Y. Wang, R. Zhang, A. Kosuga, and R. Funahashi, "Oxide thermoelectric materials: a nanostructuring approach," *Annual Review of Materials Research*, vol. 40, pp. 363–394, 2010 (English).

[20] J. He, Y. Liu, and R. Funahashi, "Oxide thermoelectrics: the challenges, progress, and outlook," *Journal of Materials Research*, vol. 26, no. 15, pp. 1762–1772, 2011.

[21] W. G. Zeier, J. Schmitt, G. Hautier et al., "Engineering half-Heusler thermoelectric materials using Zintl chemistry," *Nature Reviews Materials*, vol. 1, no. 6, p. 16032, 2016.

[22] C. Fu, S. Bai, Y. Liu et al., "Realizing high figure of merit in heavy-band p-type half-Heusler thermoelectric materials," *Nature Communications*, vol. 6, no. 1, 2015.

[23] B. Poudel, Q. Hao, Y. Ma et al., "High-thermoelectric performance of nanostructured bismuth antimony telluride bulk alloys," *Science*, vol. 320, no. 5876, pp. 634–638, 2008.

[24] S. I. Kim, K. H. Lee, H. A. Mun et al., "Dense dislocation arrays embedded in grain boundaries for high-performance bulk thermoelectrics," *Science*, vol. 348, no. 6230, pp. 109–114, 2015.

[25] G. Joshi, H. Lee, Y. Lan et al., "Enhanced thermoelectric figure-of-merit in nanostructured p-type silicon germanium bulk alloys," *Nano Letters*, vol. 8, no. 12, pp. 4670–4674, 2008.

[26] L. D. Hicks and M. S. Dresselhaus, "Effect of quantum-well structures on the thermoelectric figure of merit," *Physical Review B: Condensed Matter and Materials Physics*, vol. 47, no. 19, pp. 12727–12731, 1993 (English).

[27] L. D. Hicks and M. S. Dresselhaus, "Thermoelectric figure of merit of a one-dimensional conductor," *Physical Review B: Condensed Matter and Materials Physics*, vol. 47, no. 24, pp. 16631–16634, 1993 (English).

[28] M. S. Dresselhaus, G. Chen, M. Y. Tang et al., "New directions for low-dimensional thermoelectric materials," *Advanced Materials*, vol. 19, no. 8, pp. 1043–1053, 2007 (English).

[29] T. C. Harman, P. J. Taylor, M. P. Walsh, and B. E. LaForge, "Quantum dot superlattice thermoelectric materials and devices," *Science*, vol. 297, no. 5590, pp. 2229–2232, 2002 (English).

[30] A. I. Hochbaum, R. Chen, R. D. Delgado et al., "Enhanced thermoelectric performance of rough silicon nanowires," *Nature*, vol. 451, no. 7175, pp. 163–167, 2008 (English).

[31] A. I. Boukai, Y. Bunimovich, J. Tahir-Kheli, J.-K. Yu, W. A. Goddard III, and J. R. Heath, "Silicon nanowires as efficient thermoelectric materials," *Nature*, vol. 451, no. 7175, pp. 168–171, 2008 (English).

[32] R. Venkatasubramanian, E. Siivola, T. Colpitts, and B. O'Quinn, "Thin-film thermoelectric devices with high room-temperature figures of merit," *Nature*, vol. 413, no. 6856, pp. 597–602, 2001 (English).

[33] Y. Wang, C. Gu, and X. Ruan, "Optimization of the random multilayer structure to break the random-alloy limit of thermal conductivity," *Applied Physics Letters*, vol. 106, no. 7, pp. 73104-73104, 2015 (English).

[34] Y. Wang, H. Huang, and X. Ruan, "Decomposition of coherent and incoherent phonon conduction in superlattices and random multilayers," *Physical Review B: Condensed Matter and Materials Physics*, vol. 90, no. 16, 2014.

[35] G. Chen, *Nanoscale Energy Transport And Conversion: A Parallel Treatment of Electrons, Molecules, Phonons, and Photons*, MIT-Pappalardo Series in Mechanical Engineering, Oxford University Press, New York, NY, USA, 2005.

[36] A. A. Balandin, "Thermal properties of graphene and nanostructured carbon materials," *Nature Materials*, vol. 10, no. 8, pp. 569–581, 2011 (English).

[37] Y. Wang, A. K. Vallabhaneni, B. Qiu, and X. Ruan, "Two-dimensional thermal transport in graphene: a review of numerical modeling studies," *Nanoscale and Microscale Thermophysical Engineering*, vol. 18, no. 2, pp. 155–182, 2014.

[38] M. He, F. Qiu, and Z. Q. Lin, "Towards high-performance polymer-based thermoelectric materials," *Energy & Environmental Science*, vol. 6, no. 5, pp. 1352–1361, 2013 (English).

[39] B. Russ, A. Glaudell, J. J. Urban, M. L. Chabinyc, and R. A. Segalman, "Organic thermoelectric materials for energy harvesting and temperature control," *Nature Reviews Materials*, vol. 1, no. 10, 2016 (English).

[40] Q. Zhang, Y. Sun, W. Xu, and D. Zhu, "Organic thermoelectric materials: emerging green energy materials converting heat to

electricity directly and efficiently," *Advanced Materials*, vol. 26, no. 40, pp. 6829–6851, 2014 (English).

[41] M. Kaviany, *Heat Transfer Physics*, Cambridge University Press, New York, NY, USA, 2008.

[42] B. Huang and M. Kaviany, "Ab initio and molecular dynamics predictions for electron and phonon transport in bismuth telluride," *Physical Review B: Condensed Matter and Materials Physics*, vol. 77, no. 12, 2008 (English).

[43] C. Uher, *Materials Aspect of Thermoelectricity*, CRC Press, Taylor & Francis, Boca Raton, FL, USA, 2017.

[44] H. Kim, Z. M. Gibbs, Y. Tang, H. Wang, and G. J. Snyder, "Characterization of Lorenz number with Seebeck coefficient measurement," *APL Materials*, vol. 3, no. 4, p. 041506, 2015 (English).

[45] S. Datta, *Lessons from Nanoelectronics: A New Perspective on Transport*, Lessons from Nanoscience: A Lecture Notes Series, no. 5, World Scientific, New Jersey, NJ, USA, 2nd edition, 2017.

[46] M. Cutler and N. F. Mott, "Observation of Anderson localization in an electron gas," *Physical Review*, vol. 181, no. 3, p. 1336, 1969 (English).

[47] L. D. Zhao, H. J. Wu, S. Q. Hao et al., "All-scale hierarchical thermoelectrics: MgTe in PbTe facilitates valence band convergence and suppresses bipolar thermal transport for high performance," *Energy & Environmental Science*, vol. 6, no. 11, pp. 3346–3355, 2013 (English).

[48] Y. Pei, H. Wang, Z. M. Gibbs, A. D. LaLonde, and J. G. Snyder, "Thermopower enhancement in Pb1-xMnxTe alloys and its effect on thermoelectric efficiency," *NPG Asia Materials*, vol. 4, no. 9, 2012 (English).

[49] J. P. Heremans, B. Wiendlocha, and A. M. Chamoire, "Resonant levels in bulk thermoelectric semiconductors," *Energy & Environmental Science*, vol. 5, no. 2, pp. 5510–5530, 2012 (English).

[50] M. C. Wingert, J. Zheng, S. Kwon, and R. Chen, "Thermal transport in amorphous materials: a review," *Semiconductor Science and Technology*, vol. 31, no. 11, p. 113003, 2016 (English).

[51] Z. Lu, Y. Wang, and X. Ruan, "Metal/dielectric thermal interfacial transport considering cross-interface electron-phonon coupling: Theory, two-temperature molecular dynamics, and thermal circuit," *Physical Review B: Condensed Matter and Materials Physics*, vol. 93, no. 6, 2016.

[52] Y. Wang, Z. Lu, and X. Ruan, "First principles calculation of lattice thermal conductivity of metals considering phonon-phonon and phonon-electron scattering," *Journal of Applied Physics*, vol. 119, no. 22, 2016 (English).

[53] D. J. Sanders and D. Walton, "Effect of magnon-phonon thermal relaxation on heat transport by magnons," *Physical Review B: Condensed Matter and Materials Physics*, vol. 15, no. 3, pp. 1489–1494, 1977 (English).

[54] K. Biswas, J. He, I. D. Blum et al., "High-performance bulk thermoelectrics with all-scale hierarchical architectures," *Nature*, vol. 489, no. 7416, pp. 414–418, 2012 (English).

[55] Y. Wang, A. Vallabhaneni, J. Hu, B. Qiu, Y. P. Chen, and X. Ruan, "Phonon lateral confinement enables thermal rectification in asymmetric single-material nanostructures," *Nano Letters*, vol. 14, no. 2, pp. 592–596, 2014.

[56] Y. Wang, B. Qiu, and X. Ruan, "Edge effect on thermal transport in graphene nanoribbons: a phonon localization mechanism beyond edge roughness scattering," *Applied Physics Letters*, vol. 101, no. 1, p. 013101, 2012.

[57] P. Chakraborty, L. Cao, and Y. Wang, "Ultralow lattice thermal conductivity of the random multilayer structure with lattice imperfections," *Scientific Reports*, vol. 7, no. 1, 2017 (English).

[58] B. Qiu, Z. Tian, A. Vallabhaneni et al., "First-principles simulation of electron mean-free-path spectra and thermoelectric properties in silicon," *EPL (Europhysics Letters)*, vol. 109, no. 5, p. 57006, 2015 (English).

[59] Q. Song, T. Liu, J. Zhou, Z. Ding, and G. Chen, "Ab initio study of electron mean free paths and thermoelectric properties of lead telluride," *Materials Today Physics*, vol. 2, pp. 69–77, 2017 (English).

[60] K. Lu, L. Lu, and S. Suresh, "Strengthening materials by engineering coherent internal boundaries at the nanoscale," *Science*, vol. 324, no. 5925, pp. 349–352, 2009 (English).

[61] L. Cao and M. Koslowski, "Effect of microstructural uncertainty on the yield stress of nanocrystalline nickel," *Acta Materialia*, vol. 61, no. 4, pp. 1413–1420, 2013 (English).

[62] L. Cao and M. Koslowski, "Rate-limited plastic deformation in nanocrystalline Ni," *Journal of Applied Physics*, vol. 117, no. 24, 2015 (English).

[63] G. Li, U. Aydemir, M. Wood et al., "Mechanical properties of thermoelectric lanthanum telluride from quantum mechanics," *Journal of Physics D: Applied Physics*, vol. 50, no. 27, p. 274002, 2017 (English).

[64] R. He, S. Gahlawat, C. Guo et al., "Studies on mechanical properties of thermoelectric materials by nanoindentation," *Physica Status Solidi (a)—Applications and Materials Science*, vol. 212, no. 10, pp. 2191–2195, 2015 (English).

[65] G. Li, S. I. Morozov, Q. Zhang, Q. An, P. Zhai, and G. J. Snyder, "Enhanced strength through nanotwinning in the thermoelectric semiconductor InSb," *Physical Review Letters*, vol. 119, no. 21, 2017 (English).

[66] M. G. Lavrentev, V. B. Osvenskii, Y. N. Parkhomenko et al., "Improved mechanical properties of thermoelectric (Bi0.2Sb0.8)(2)Te-3 by nanostructuring," *APL Materials*, vol. 4, no. 10, p. 104807, 2016 (English).

[67] M. A. Meyers, A. Mishra, and D. J. Benson, "Mechanical properties of nanocrystalline materials," *Progress in Materials Science*, vol. 51, no. 4, pp. 427–556, 2006 (English).

[68] L. Cao, A. Hunter, I. J. Beyerlein, and M. Koslowski, "The role of partial mediated slip during quasi-static deformation of 3D nanocrystalline metals," *Journal of the Mechanics and Physics of Solids*, vol. 78, pp. 415–426, 2015 (English).

[69] L. Cao, A. Sengupta, D. Pantuso, and M. Koslowski, "Effect of texture and grain size on the residual stress of nanocrystalline thin films," *Modelling and Simulation in Materials Science and Engineering*, vol. 25, no. 7, 2017 (English).

[70] S. Perumal, S. Roychowdhury, D. S. Negi, R. Datta, and K. Biswas, "High thermoelectric performance and enhanced mechanical stability of p-type Ge1-xSbxTe," *Chemistry of Materials*, vol. 27, no. 20, pp. 7171–7178, 2015 (English).

[71] X. Shi, H. Chen, F. Hao et al., "Room-temperature ductile inorganic semiconductor," *Nature Materials*, vol. 17, no. 5, pp. 421–426, 2018.

[72] K. I. Bolotin, K. J. Sikes, Z. Jiang et al., "Ultrahigh electron mobility in suspended graphene," *Solid State Communications*, vol. 146, no. 9-10, pp. 351–355, 2008.

[73] Y. Ouyang and J. Guo, "A theoretical study on thermoelectric properties of graphene nanoribbons," *Applied Physics Letters*, vol. 94, no. 26, 2009 (English).

[74] Y. Anno, Y. Imakita, K. Takei, S. Akita, and T. Arie, "Enhancement of graphene thermoelectric performance through defect engineering," *2D Materials*, vol. 4, no. 2, p. 025019, 2017.

[75] H. Sevinçli and G. Cuniberti, "Enhanced thermoelectric figure of merit in edge-disordered zigzag graphene nanoribbons," *Physical Review B: Condensed Matter and Materials Physics*, vol. 81, no. 11, 2010 (English).

[76] S. Chen, Q. Wu, C. Mishra et al., "Thermal conductivity of isotopically modified graphene," *Nature Materials*, vol. 11, no. 3, pp. 203–207, 2012 (English).

[77] J. Hu, S. Schiffli, A. Vallabhaneni, X. Ruan, and Y. P. Chen, "Tuning the thermal conductivity of graphene nanoribbons by edge passivation and isotope engineering: a molecular dynamics study," *Applied Physics Letters*, vol. 97, no. 13, 2010 (English).

[78] Y. Wang and X. Ruan, "Role of EDGE chirality and isotope doping in thermal transport and thermal rectification in graphene nanoribbons," in *Proceedings of the ASME 2011 International Mechanical Engineering Congress and Exposition (IMECE '11)*, pp. 315–322, November 2011.

[79] Y. Wang, S. Chen, and X. Ruan, "Tunable thermal rectification in graphene nanoribbons through defect engineering: a molecular dynamics study," *Applied Physics Letters*, vol. 100, no. 16, p. 163101, 2012.

[80] M. Noshin, A. I. Khan, I. A. Navid, H. M. A. Uddin, and S. Subrina, "Impact of vacancies on the thermal conductivity of graphene nanoribbons: a molecular dynamics simulation study," *AIP Advances*, vol. 7, no. 1, 2017 (English).

[81] J. Haskins, A. Kinaci, C. Sevik, H. Sevinçli, G. Cuniberti, and T. Çağin, "Control of thermal and electronic transport in defect-engineered graphene nanoribbons," *ACS Nano*, vol. 5, no. 5, pp. 3779–3787, 2011 (English).

[82] Z. G. Fthenakis and D. Tománek, "Computational study of the thermal conductivity in defective carbon nanostructures," *Physical Review B: Condensed Matter and Materials Physics*, vol. 86, no. 12, 2012 (English).

[83] T. Feng and X. Ruan, "Ultra-low thermal conductivity in graphene nanomesh," *Carbon*, vol. 101, pp. 107–113, 2016 (English).

[84] J.-K. Yu, S. Mitrovic, D. Tham, J. Varghese, and J. R. Heath, "Reduction of thermal conductivity in phononic nanomesh structures," *Nature Nanotechnology*, vol. 5, no. 10, pp. 718–721, 2010 (English).

[85] W. J. Evans, L. Hu, and P. Keblinski, "Thermal conductivity of graphene ribbons from equilibrium molecular dynamics: effect of ribbon width, edge roughness, and hydrogen termination," *Applied Physics Letters*, vol. 96, no. 20, 2010 (English).

[86] Z. Aksamija and I. Knezevic, "Anisotropy and edge roughness scattering in the lattice thermal conductivity of graphene nanoribbons," *Fullerenes, Nanotubes, and Carbon Nanostructures—219th Ecs Meeting*, vol. 35, no. 25, pp. 195–200, 2011 (English).

[87] Z. Aksamija and I. Knezevic, "Lattice thermal conductivity of graphene nanoribbons: anisotropy and edge roughness scattering," *Applied Physics Letters*, vol. 98, no. 14, 2011 (English).

[88] P. S. E. Yeo, M. B. Sullivan, K. P. Loh, and C. K. Gan, "First-principles study of the thermoelectric properties of strained graphene nanoribbons," *Journal of Materials Chemistry A*, vol. 1, no. 36, pp. 10762–10767, 2013.

[89] L. Hu and D. Maroudas, "Thermal transport properties of graphene nanomeshes," *Journal of Applied Physics*, vol. 116, no. 18, p. 184304, 2014.

[90] I. Jung, H. Y. Jang, J. Moon, and S. Park, "Fabrication of a graphene nanomesh using a platinum nano-network as a pattern mask," *Nanoscale*, vol. 6, no. 12, pp. 6482–6486, 2014 (English).

[91] J. Bai, X. Zhong, S. Jiang, Y. Huang, and X. Duan, "Graphene nanomesh," *Nature Nanotechnology*, vol. 5, no. 3, pp. 190–194, 2010.

[92] P. E. Hopkins, C. M. Reinke, M. F. Su et al., "Reduction in the thermal conductivity of single crystalline silicon by phononic crystal patterning," *Nano Letters*, vol. 11, no. 1, pp. 107–112, 2011 (English).

[93] J. Carrete, N. Mingo, and S. Curtarolo, "Low thermal conductivity and triaxial phononic anisotropy of SnSe," *Applied Physics Letters*, vol. 105, no. 10, 2014 (English).

[94] S. Alaie, D. F. Goettler, M. Su, Z. C. Leseman, C. M. Reinke, and I. El-Kady, "Thermal transport in phononic crystals and the observation of coherent phonon scattering at room temperature," *Nature Communications*, vol. 6, 2015 (English).

[95] M. V. Simkin and G. D. Mahan, "Minimum thermal conductivity of superlattices," *Physical Review Letters*, vol. 84, no. 5, pp. 927–930, 2000 (English).

[96] J. Tang, H.-T. Wang, D. H. Lee et al., "Holey silicon as an efficient thermoelectric material," *Nano Letters*, vol. 10, no. 10, pp. 4279–4283, 2010.

[97] H. Sadeghi, S. Sangtarash, and C. J. Lambert, "Enhancing the thermoelectric figure of merit in engineered graphene nanoribbons," *Beilstein Journal of Nanotechnology*, vol. 6, no. 1, pp. 1176–1182, 2015.

[98] M. Yarifard, J. Davoodi, and H. Rafii-Tabar, "In-plane thermal conductivity of graphene nanomesh: A molecular dynamics study," *Computational Materials Science*, vol. 111, pp. 247–251, 2016.

[99] Q. Hao, "Effective medium formulation for phonon transport analysis of nanograined polycrystals," *Journal of Applied Physics*, vol. 111, no. 1, 2012.

[100] L. Jiao, L. Zhang, X. Wang, G. Diankov, and H. Dai, "Narrow graphene nanoribbons from carbon nanotubes," *Nature*, vol. 458, no. 7240, pp. 877–880, 2009.

[101] J. Bai, X. Duan, and Y. Huang, "Rational fabrication of graphene nanoribbons using a nanowire etch mask," *Nano Letters*, vol. 9, no. 5, pp. 2083–2087, 2009.

[102] J. Cai, P. Ruffieux, R. Jaafar et al., "Atomically precise bottom-up fabrication of graphene nanoribbons," *Nature*, vol. 466, no. 7305, pp. 470–473, 2010.

[103] A. Radocea, T. Sun, T. H. Vo, A. Sinitskii, N. R. Aluru, and J. W. Lyding, "Solution-synthesized chevron graphene nanoribbons exfoliated onto H:Si(100)," *Nano Letters*, vol. 17, no. 1, pp. 170–178, 2017 (English).

[104] L. Liang, C.-S. Eduardo, C.-G. Eduardo, and M. Vincent, "Enhanced thermoelectric figure of merit in assembled graphene nanoribbons," *Physical Review B: Condensed Matter and Materials Physics*, vol. 86, p. 115438, 2012.

[105] W. Huang, J.-S. Wang, and G. Liang, "Theoretical study on thermoelectric properties of kinked graphene nanoribbons," *Physical Review B: Condensed Matter and Materials Physics*, vol. 84, no. 4, 2011 (English).

[106] F. Mazzamuto, V. Hung Nguyen, Y. Apertet et al., "Enhanced thermoelectric properties in graphene nanoribbons by resonant tunneling of electrons," *Physical Review B: Condensed Matter and Materials Physics*, vol. 83, no. 23, 2011 (English).

[107] Y. Chen, T. Jayasekera, A. Calzolari, K. W. Kim, and M. B. Nardelli, "Thermoelectric properties of graphene nanoribbons, junctions and superlattices," *Journal of Physics: Condensed Matter*, vol. 22, no. 37, p. 372202, 2010.

[108] H. Sevinçli, C. Sevik, T. Çain, and G. Cuniberti, "A bottom-up route to enhance thermoelectric figures of merit in graphene nanoribbons," *Scientific Reports*, vol. 3, article 1228, 2013 (English).

[109] A. M. Rao, X. Ji, and T. M. Tritt, "Properties of nanostructured one-dimensional and composite thermoelectric materials," *MRS Bulletin*, vol. 31, no. 3, pp. 218–223, 2006 (English).

[110] W. Zhou, J. Vavro, N. M. Nemes et al., "Charge transfer and Fermi level shift in p-doped single-walled carbon nanotubes," *Physical Review B: Condensed Matter and Materials Physics*, vol. 71, no. 20, 2005 (English).

[111] Y. Nonoguchi, K. Ohashi, R. Kanazawa et al., "Systematic conversion of single walled carbon nanotubes into n-type thermoelectric materials by molecular dopants," *Scientific Reports*, vol. 3, no. 1, 2013 (English).

[112] Y. Nonoguchi, K. Hata, and T. Kawai, "Dispersion of synthetic mos2 flakes and their spontaneous adsorption on single-walled carbon nanotubes," *ChemPlusChem*, vol. 80, no. 7, pp. 1158–1163, 2015 (English).

[113] D. Hayashi, T. Ueda, Y. Nakai et al., "Thermoelectric properties of single-wall carbon nanotube films: effects of diameter and wet environment," *Applied Physics Express*, vol. 9, no. 2, p. 025102, 2016 (English).

[114] Y. Nonoguchi, M. Nakano, T. Murayama et al., "Simple salt-coordinated n-type nanocarbon materials stable in air," *Advanced Functional Materials*, vol. 26, no. 18, pp. 3021–3028, 2016 (English).

[115] W. Zhou, Q. Fan, Q. Zhang et al., "Ultrahigh-power-factor carbon nanotubes and an ingenious strategy for thermoelectric performance evaluation," *Small*, vol. 12, no. 25, pp. 3407–3414, 2016 (English).

[116] D. Hayashi, Y. Nakai, H. Kyakuno et al., "Improvement of thermoelectric performance of single-wall carbon nanotubes by heavy doping: effect of one-dimensional band multiplicity," *Applied Physics Express*, vol. 9, no. 12, p. 125103, 2016 (English).

[117] Y. Nonoguchi, Y. Iihara, K. Ohashi, T. Murayama, and T. Kawai, "Air-tolerant fabrication and enhanced thermoelectric performance of n-type single-walled carbon nanotubes encapsulating 1,1′-Bis(diphenylphosphino)ferrocene," *Chemistry*, vol. 11, no. 17, pp. 2423–2427, 2016 (English).

[118] W. Zhou, Q. Fan, Q. Zhang et al., "High-performance and compact-designed flexible thermoelectric modules enabled by a reticulate carbon nanotube architecture," *Nature Communications*, vol. 8, p. 14886, 2017 (English).

[119] Y. Nonoguchi, S. Sudo, A. Tani et al., "Solvent basicity promotes the hydride-mediated electron transfer doping of carbon nanotubes," *Chemical Communications*, vol. 53, no. 74, pp. 10259–10262, 2017 (English).

[120] J. Choi, Y. Jung, S. J. Yang et al., "Flexible and robust thermoelectric generators based on all-carbon nanotube yarn without metal electrodes," *ACS Nano*, vol. 11, no. 8, pp. 7608–7614, 2017 (English).

[121] Y. Nakashima, N. Nakashima, and T. Fujigaya, "Development of air-stable n-type single-walled carbon nanotubes by doping with 2-(2-methoxyphenyl)-1,3-dimethyl-2,3-dihydro-1H-benzo[d]imidazole and their thermoelectric properties," *Synthetic Metals*, vol. 225, pp. 76–80, 2017 (English).

[122] Y. Nakai, K. Honda, K. Yanagi et al., "Giant Seebeck coefficient in semiconducting single-wall carbon nanotube film," *Applied Physics Express*, vol. 7, no. 2, p. 025103, 2014 (English).

[123] M. Piao, M. Joo, J. Na et al., "Effect of intertube junctions on the thermoelectric power of monodispersed single walled carbon nanotube networks," *The Journal of Physical Chemistry C*, vol. 118, no. 46, pp. 26454–26461, 2014 (English).

[124] A. D. Avery, B. H. Zhou, J. Lee et al., "Tailored semiconducting carbon nanotube networks with enhanced thermoelectric properties," *Nature Energy*, vol. 1, no. 4, p. 16033, 2016 (English).

[125] B. Norton-Baker, R. Ihly, I. E. Gould et al., "Polymer-free carbon nanotube thermoelectrics with improved charge carrier transport and power factor," *ACS Energy Letters*, vol. 1, no. 6, pp. 1212–1220, 2016 (English).

[126] B. A. MacLeod, N. J. Stanton, I. E. Gould et al., "Large n- and p-type thermoelectric power factors from doped semiconducting single-walled carbon nanotube thin films," *Energy & Environmental Science*, vol. 10, no. 10, pp. 2168–2179, 2017 (English).

[127] Y. Sun, S. R. Wilson, and D. I. Schuster, "High dissolution and strong light emission of carbon nanotubes in aromatic amine solvents," *Journal of the American Chemical Society*, vol. 123, no. 22, pp. 5348-5349, 2001 (English).

[128] T. W. Ebbesen, H. J. Lezec, H. Hiura, J. W. Bennett, H. F. Ghaemi, and T. Thio, "Electrical conductivity of individual carbon nanotubes," *Nature*, vol. 382, pp. 54–56, 1996 (English).

[129] Y. Ando, X. Zhao, H. Shimoyama, G. Sakai, and K. Kaneto, "Physical properties of multiwalled carbon nanotubes," *International Journal of Inorganic Materials*, vol. 1, no. 1, pp. 77–82, 1999 (English).

[130] G. Basile, C. Bernardin, and S. Olla, "Momentum conserving model with anomalous thermal conductivity in low dimensional systems," *Physical Review Letters*, vol. 96, no. 20, p. 204303, 2006.

[131] S. Lepri, R. Livi, and A. Politi, "Thermal conduction in classical low-dimensional lattices," *Physics Reports*, vol. 377, no. 1, pp. 1–80, 2003.

[132] O. Narayan and S. Ramaswamy, "Anomalous heat conduction in one-dimensional momentum-conserving systems," *Physical Review Letters*, vol. 89, no. 20, 2002 (English).

[133] L. Wang, B. Hu, and B. Li, "Logarithmic divergent thermal conductivity in two-dimensional nonlinear lattices," *Physical Review E: Statistical, Nonlinear, and Soft Matter Physics*, vol. 86, no. 4, 2012 (English).

[134] V. Lee, C. Wu, Z. Lou, W. Lee, and C. Chang, "Divergent and ultrahigh thermal conductivity in millimeter-long nanotubes," *Physical Review Letters*, vol. 118, no. 13, 2017 (English).

[135] X. Xu, L. F. Pereira, Y. Wang et al., "Length-dependent thermal conductivity in suspended single-layer graphene," *Nature Communications*, vol. 5, no. 1, 2014 (English).

[136] Q. Li, K. Takahashi, and X. Zhang, "Comment on 'divergent and ultrahigh thermal conductivity in millimeter-long nanotubes'," *Physical Review Letters*, vol. 119, no. 17, 2017.

[137] G. U. Sumanasekera, C. K. W. Adu, S. Fang, and P. C. Eklund, "Effects of gas adsorption and collisions on electrical transport in single-walled carbon nanotubes," *Physical Review Letters*, vol. 85, no. 5, pp. 1096–1099, 2000.

[138] B. Sadanadan, T. Savage, S. Bhattacharya et al., "Synthesis and thermoelectric power of nitrogen-doped carbon nanotubes," *Journal of Nanoscience and Nanotechnology*, vol. 3, no. 1-2, pp. 99–103, 2003.

[139] K. McGuire, N. Gothard, P. L. Gai, M. S. Dresselhaus, G. Sumanasekera, and A. M. Rao, "Synthesis and Raman characterization of boron-doped single-walled carbon nanotubes," *Carbon*, vol. 43, no. 2, pp. 219–227, 2005.

[140] J. P. Small, K. M. Perez, and P. Kim, "Modulation of thermoelectric power of individual carbon nanotubes," *Physical Review Letters*, vol. 91, no. 25, 2003.

[141] P. Kim, L. Shi, A. Majumdar, and P. L. McEuen, "Thermal transport measurements of individual multiwalled nanotubes," *Physical Review Letters*, vol. 87, no. 21, pp. 215502–215502-4, 2001 (English).

[142] C. Yu, L. Shi, Z. Yao, D. Li, and A. Majumdar, "Thermal conductance and thermopower of an individual single-wall carbon nanotube," *Nano Letters*, vol. 5, no. 9, pp. 1842–1846, 2005 (English).

[143] X. Tan, H. Liu, Y. Wen et al., "Optimizing the thermoelectric performance of zigzag and chiral carbon nanotubes," *Nanoscale Research Letters*, vol. 7, no. 1, p. 116, 2012.

[144] B. Qiu, Y. Wang, Q. Zhao, and X. Ruan, "The effects of diameter and chirality on the thermal transport in free-standing and supported carbon-nanotubes," *Applied Physics Letters*, vol. 100, no. 23, p. 233105, 2012.

[145] L. Lindsay, D. A. Broido, and N. Mingo, "Diameter dependence of carbon nanotube thermal conductivity and extension to the graphene limit," *Physical Review B: Condensed Matter and Materials Physics*, vol. 82, no. 16, 2010 (English).

[146] R. S. Prasher, X. J. Hu, Y. Chalopin et al., "Turning carbon nanotubes from exceptional heat conductors into insulators," *Physical Review Letters*, vol. 102, no. 10, p. 105901, 2009.

[147] T. Miao, W. Ma, X. Zhang, J. Wei, and J. Sun, "Significantly enhanced thermoelectric properties of ultralong double-walled carbon nanotube bundle," *Applied Physics Letters*, vol. 102, no. 5, p. 053105, 2013.

[148] M. T. Pettes and L. Shi, "Thermal and structural characterizations of individual single-, double-, and multi-walled carbon nanotubes," *Advanced Functional Materials*, vol. 19, no. 24, pp. 3918–3925, 2009.

[149] A. E. Aliev, M. H. Lima, E. M. Silverman, and R. H. Baughman, "Thermal conductivity of multi-walled carbon nanotube sheets: radiation losses and quenching of phonon modes," *Nanotechnology*, vol. 21, no. 3, 2010 (English).

[150] T. Kodama, M. Ohnishi, W. Park et al., "Modulation of thermal and thermoelectric transport in individual carbon nanotubes by fullerene encapsulation," *Nature Materials*, vol. 16, no. 9, pp. 892–897, 2017.

[151] J. Vavro, M. C. Llaguno, B. C. Satishkumar, D. E. Luzzi, and J. E. Fischer, "Electrical and thermal properties of C60-filled single-wall carbon nanotubes," *Applied Physics Letters*, vol. 80, no. 8, pp. 1450–1452, 2002 (English).

[152] T. Fukumaru, T. Fujigaya, and N. Nakashima, "Development of n-type cobaltocene-encapsulated carbon nanotubes with remarkable thermoelectric property," *Scientific Reports*, vol. 5, 2015 (English).

[153] L.-J. Li, A. N. Khlobystov, J. G. Wiltshire, G. A. D. Briggs, and R. J. Nicholas, "Diameter-selective encapsulation of metallocenes in single-walled carbon nanotubes," *Nature Materials*, vol. 4, no. 6, pp. 481–485, 2005 (English).

[154] S. K. Yee, J. A. Malen, A. Majumdar, and R. A. Segalman, "Thermoelectricity in fullerene-metal heterojunctions," *Nano Letters*, vol. 11, no. 10, pp. 4089–4094, 2011 (English).

[155] C. Evangeli, K. Gillemot, E. Leary et al., "Engineering the thermopower of C60 molecular junctions," *Nano Letters*, vol. 13, no. 5, pp. 2141–2145, 2013 (English).

[156] S. K. Lee, T. Ohto, R. Yamada, and H. Tada, "Thermopower of benzenedithiol and C60 molecular junctions with Ni and Au Electrodes," *Nano Letters*, vol. 14, no. 9, pp. 5276–5280, 2014.

[157] Y. Kim, W. Jeong, K. Kim, W. Lee, and P. Reddy, "Electrostatic control of thermoelectricity in molecular junctions," *Nature Nanotechnology*, vol. 9, no. 11, pp. 881–885, 2014 (English).

[158] L. Rincón-García, A. K. Ismael, C. Evangeli et al., "Molecular design and control of fullerene-based bi-thermoelectric materials," *Nature Materials*, vol. 15, no. 3, pp. 289–293, 2016 (English).

[159] P. Gehring, A. Harzheim, J. Spièce et al., "Field-effect control of graphene-fullerene thermoelectric nanodevices," *Nano Letters*, vol. 17, no. 11, pp. 7055–7061, 2017 (English).

[160] D. Malko, C. Neiss, F. Viñes, and A. Görling, "Competition for graphene: graphynes with direction-dependent dirac cones," *Physical Review Letters*, vol. 108, no. 8, 2012 (English).

[161] S. W. Cranford and M. J. Buehler, "Mechanical properties of graphyne," *Carbon*, vol. 49, no. 13, pp. 4111–4121, 2011 (English).

[162] K. Srinivasu and S. K. Ghosh, "Graphyne and graphdiyne: promising materials for nanoelectronics and energy storage applications," *The Journal of Physical Chemistry C*, vol. 116, no. 9, pp. 5951–5956, 2012 (English).

[163] T. Ouyang, H. Xiao, Y. Xie, X. Wei, Y. Chen, and J. Zhong, "Thermoelectric properties of gamma-graphyne nanoribbons and nanojunctions," *Journal of Applied Physics*, vol. 114, no. 7, 2013 (English).

[164] W. X. Zhou and K. Q. Chen, "Enhancement of thermoelectric performance in beta-graphyne nanoribbons by suppressing phononic thermal conductance," *Carbon*, vol. 85, pp. 24–27, 2015 (English).

[165] G. D. Mahan and J. O. Sofo, "The best thermoelectric," *Proceedings of the National Acadamy of Sciences of the United States of America*, vol. 93, no. 15, pp. 7436–7439, 1996 (English).

[166] Y. Yan, Q. Liang, H. Zhao, and C. Wu, "Thermoelectric properties of hexagonal graphene quantum dots," *Physics Letters A*, vol. 376, no. 12-13, pp. 1154–1158, 2012.

[167] Y. Liu, X. Shao, T. Shao et al., "Gate-enhanced thermoelectric effects in all-carbon quantum devices," *Carbon*, vol. 109, pp. 411–417, 2016 (English).

[168] B.-Y. Cao, W.-J. Yao, and Z.-Q. Ye, "Networked nanoconstrictions: An effective route to tuning the thermal transport properties of graphene," *Carbon*, vol. 96, pp. 711–719, 2016.

[169] Y. Wang, Multiscale simulations of thermal transport in graphene-based materials and across metal-semiconductor interfaces, 2016.

[170] V. Hung Nguyen, M. C. Nguyen, H.-V. Nguyen, J. Saint-Martin, and P. Dollfus, "Enhanced thermoelectric figure of merit in vertical graphene junctions," *Applied Physics Letters*, vol. 105, no. 13, 2014 (English).

[171] B. Zhou, Y. Gao, B. Zhou, Y. Yao, G. Zhou, and M. Hu, "Enhanced thermoelectric properties of the AGNR–GYNR heterojunctions," *Physics Letters A*, vol. 381, no. 44, pp. 3766–3772, 2017 (English).

[172] C. Yu, K. Choi, L. Yin, and J. C. Grunlan, "Light-weight flexible carbon nanotube based organic composites with large thermoelectric power factors," *ACS Nano*, vol. 5, no. 10, pp. 7885–7892, 2011.

[173] K. T. Kim, S. Y. Choi, E. H. Shin et al., "The influence of CNTs on the thermoelectric properties of a CNT/Bi_2Te_3 composite," *Carbon*, vol. 52, pp. 541–549, 2013 (English).

[174] H. Mishra, B. A. Cola, V. Rawat et al., "Thermomechanical and thermal contact characteristics of bismuth telluride films electrodeposited on carbon nanotube arrays," *Advanced Materials*, vol. 21, no. 42, pp. 4280–4283, 2009 (English).

[175] G.-D. Zhan, J. D. Kuntz, A. K. Mukherjee, P. Zhu, and K. Koumoto, "Thermoelectric properties of carbon nanotube/ceramic nanocomposites," *Scripta Materialia*, vol. 54, no. 1, pp. 77–82, 2006 (English).

[176] Y. Yokomizo and J. Nakamura, "Giant Seebeck coefficient of the graphene/h-BN superlattices," *Applied Physics Letters*, vol. 103, no. 11, p. 113901, 2013.

[177] J. Shiomi and S. Maruyama, "Heat conduction of single-walled carbon nanotube isotope superlattice structures: a molecular dynamics study," *Physical Review B: Condensed Matter and Materials Physics*, vol. 74, no. 15, p. 155401, 2006.

[178] X. Mu, T. Zhang, D. B. Go, and T. Luo, "Coherent and incoherent phonon thermal transport in isotopically modified graphene superlattices," *Carbon*, vol. 83, pp. 208–216, 2015 (English).

[179] Y. Choi, Y. Kim, S. Park et al., "Effect of the carbon nanotube type on the thermoelectric properties of CNT/Nafion nanocomposites," *Organic Electronics*, vol. 12, no. 12, pp. 2120–2125, 2011 (English).

[180] Y. Hiroshige, M. Ookawa, and N. Toshima, "High thermoelectric performance of poly(2,5-dimethoxyphenylenevinylene) and its derivatives," *Synthetic Metals*, vol. 156, no. 21–24, pp. 1341–1347, 2006 (English).

[181] J. Luo, G. Cerretti, B. Krause et al., "Polypropylene-based melt mixed composites with singlewalled carbon nanotubes for thermoelectric applications: switching from p-type to n-type by the addition of polyethylene glycol," *Polymer Journal*, vol. 108, pp. 513–520, 2017 (English).

[182] Q. Yao, L. Chen, W. Zhang, S. Liufu, and X. Chen, "Enhanced thermoelectric performance of single-walled carbon nanotubes/polyaniline hybrid nanocomposites," *ACS Nano*, vol. 4, no. 4, pp. 2445–2451, 2010 (English).

[183] L. Wang, Q. Yao, W. Shi, S. Qu, and L. Chen, "Engineering carrier scattering at the interfaces in polyaniline based nanocomposites for high thermoelectric performances," *Materials Chemistry Frontiers*, vol. 1, no. 4, pp. 741–748, 2017 (English).

[184] K. Zhang, M. Davis, J. Qiu, L. Hope-Weeks, and S. Wang, "Thermoelectric properties of porous multi-walled carbon nanotube/polyaniline core/shell nanocomposites," *Nanotechnology*, vol. 23, no. 38, 2012 (English).

[185] C. Meng, C. Liu, and S. Fan, "A promising approach to enhanced thermoelectric properties using carbon nanotube networks," *Advanced Materials*, vol. 22, no. 4, pp. 535–539, 2010 (English).

[186] Q. Wang, Q. Yao, J. Chang, and L. Chen, "Enhanced thermoelectric properties of CNT/PANI composite nanofibers by highly orienting the arrangement of polymer chains," *Journal of Materials Chemistry*, vol. 22, no. 34, pp. 17612–17618, 2012 (English).

[187] Q. Zhang, W. Wang, J. Li et al., "Preparation and thermoelectric properties of multi-walled carbon nanotube/polyaniline hybrid nanocomposites," *Journal of Materials Chemistry A*, vol. 1, no. 39, pp. 12109–12114, 2013 (English).

[188] H. Wang, S.-I. Yi, X. Pu, and C. Yu, "Simultaneously improving electrical conductivity and thermopower of polyaniline composites by utilizing carbon nanotubes as high mobility conduits," *ACS Applied Materials & Interfaces*, vol. 7, no. 18, pp. 9589–9597, 2015 (English).

[189] G.-H. Kim, L. Shao, K. Zhang, and K. P. Pipe, "Engineered doping of organic semiconductors for enhanced thermoelectric efficiency," *Nature Materials*, vol. 12, no. 8, pp. 719–723, 2013 (English).

[190] G. P. Moriarty, S. De, P. J. King et al., "Thermoelectric behavior of organic thin film nanocomposites," *Journal of Polymer Science Part B: Polymer Physics*, vol. 51, no. 2, pp. 119–123, 2013 (English).

[191] G. P. Moriarty, K. Briggs, B. Stevens, C. Yu, and J. C. Grunlan, "Fully organic nanocomposites with high thermoelectric power factors by using a dual-stabilizer preparation," *Energy Technology*, vol. 1, no. 4, pp. 265–272, 2013 (English).

[192] H. Song, C. Liu, J. Xu, Q. Jiang, and H. Shi, "Fabrication of a layered nanostructure PEDOT:PSS/SWCNTs composite and its thermoelectric performance," *RSC Advances*, vol. 3, no. 44, pp. 22065–22071, 2013 (English).

[193] W. Lee, Y. H. Kang, J. Y. Lee, K.-S. Jang, and S. Y. Cho, "Improving the thermoelectric power factor of CNT/PEDOT:PSS nanocomposite films by ethylene glycol treatment," *RSC Advances*, vol. 6, no. 58, pp. 53339–53344, 2016 (English).

[194] L. Liang, C. Gao, G. Chen, and C.-Y. Guo, "Large-area, stretchable, super flexible and mechanically stable thermoelectric films of polymer/carbon nanotube composites," *Journal of Materials Chemistry C*, vol. 4, no. 3, pp. 526–532, 2016 (English).

[195] J. Wang, K. Cai, S. Shen, and J. Yin, "Preparation and thermoelectric properties of multi-walled carbon nanotubes/polypyrrole composites," *Synthetic Metals*, vol. 195, pp. 132–136, 2014 (English).

[196] L. Liang, G. Chen, and C.-Y. Guo, "Enhanced thermoelectric performance by self-assembled layered morphology of polypyrrole nanowire/single-walled carbon nanotube composites," *Composites Science and Technology*, vol. 129, pp. 130–136, 2016.

[197] R. Yue and J. Xu, "Poly(3,4-ethylenedioxythiophene) as promising organic thermoelectric materials: a mini-review," *Synthetic Metals*, vol. 162, no. 11-12, pp. 912–917, 2012 (English).

[198] Y. Du, S. Z. Shen, K. Cai, and P. S. Casey, "Research progress on polymer—inorganic thermoelectric nanocomposite materials," *Progress in Polymer Science*, vol. 37, no. 6, pp. 820–841, 2012 (English).

[199] W. Lee, C. T. Hong, O. H. Kwon et al., "Enhanced thermoelectric performance of bar-coated SWCNT/P3HT thin films," *Acs Applied Materials & Interfaces*, vol. 7, no. 12, pp. 6550–6556, 2015 (English).

[200] L. Wang, X. Jia, D. Wang, G. Zhu, and J. Li, "Preparation and thermoelectric properties of polythiophene/multiwalled carbon nanotube composites," *Synthetic Metals*, vol. 181, pp. 79–85, 2013 (English).

[201] F. Rivadulla, C. Mateo-Mateo, and M. A. Correa-Duarte, "Layer-by-layer polymer coating of carbon nanotubes: tuning of electrical conductivity in random networks," *Journal of the American Chemical Society*, vol. 132, no. 11, pp. 3751–3755, 2010 (English).

[202] C. Cho, B. Stevens, J.-H. Hsu et al., "Completely organic multilayer thin film with thermoelectric power factor rivaling inorganic tellurides," *Advanced Materials*, vol. 27, no. 19, pp. 2996–3001, 2015 (English).

[203] C. Cho, K. L. Wallace, P. Tzeng, J.-H. Hsu, C. Yu, and J. C. Grunlan, "Outstanding low temperature thermoelectric power factor from completely organic thin films enabled by multidimensional conjugated nanomaterials," *Advanced Energy Materials*, vol. 6, no. 7, 2016 (English).

[204] C. Yu, Y. S. Kim, D. Kim, and J. C. Grunlan, "Thermoelectric behavior of segregated-network polymer nanocomposites," *Nano Letters*, vol. 8, no. 12, pp. 4428–4432, 2008.

[205] D. Kim, Y. Kim, K. Choi, J. C. Grunlan, and C. Yu, "Improved thermoelectric behavior of nanotube-filled polymer composites with poly(3,4-ethylenedioxythiophene)poly(styrenesulfonate)," *ACS Nano*, vol. 4, no. 1, pp. 513–523, 2010 (English).

[206] G. P. Moriarty, J. N. Wheeler, C. Yu, and J. C. Grunlan, "Increasing the thermoelectric power factor of polymer composites using a semiconducting stabilizer for carbon nanotubes," *Carbon*, vol. 50, no. 3, pp. 885–895, 2012 (English).

[207] G. H. Kim, D. H. Hwang, and S. I. Woo, "Thermoelectric properties of nanocomposite thin films prepared with poly(3,4-ethylenedioxythiophene)poly(styrenesulfonate) and graphene," *Physical Chemistry Chemical Physics*, vol. 14, no. 10, pp. 3530–3536, 2012.

[208] Q. Yao, Q. Wang, L. Wang, and L. Chen, "Abnormally enhanced thermoelectric transport properties of SWNT/PANI hybrid films by the strengthened PANI molecular ordering," *Energy & Environmental Science*, vol. 7, no. 11, pp. 3801–3807, 2014 (English).

[209] X. Gui, J. Wei, K. Wang et al., "Carbon nanotube sponges," *Advanced Materials*, vol. 22, no. 5, pp. 617–621, 2010.

[210] J. Chen et al., "Superlow thermal conductivity 3D carbon nanotube network for thermoelectric applications," *ACS Applied Materials & Interfaces*, vol. 4, no. 1, pp. 81–86, 2011.

[211] C. T. Hong, W. Lee, Y. H. Kang et al., "Effective doping by spin-coating and enhanced thermoelectric power factors in SWCNT/P3HT hybrid films," *Journal of Materials Chemistry A*, vol. 3, no. 23, pp. 12314–12319, 2015 (English).

[212] J. Liu, J. Sun, and L. Gao, "Flexible single-walled carbon nanotubes/polyaniline composite films and their enhanced thermoelectric properties," *Nanoscale*, vol. 3, no. 9, pp. 3616–3619, 2011.

[213] H. Yan and K. Kou, "Enhanced thermoelectric properties in polyaniline composites with polyaniline-coated carbon nanotubes," *Journal of Materials Science*, vol. 49, no. 3, pp. 1222–1228, 2014.

[214] L. Wang, Q. Yao, J. Xiao et al., "Engineered molecular chain ordering in single-walled carbon nanotubes/polyaniline composite films for high-performance organic thermoelectric materials," *Chemistry*, vol. 11, no. 12, pp. 1804–1810, 2016.

[215] C. Bounioux, P. Diaz-Chao, M. Campoy-Quiles et al., "Thermoelectric composites of poly (3-hexylthiophene) and carbon nanotubes with a large power factor," *Energy & Environmental Science*, vol. 6, no. 3, pp. 918–925, 2013.

[216] C. T. Hong, Y. H. Kang, J. Ryu, S. Y. Cho, and K.-S. Jang, "Spray-printed CNT/P3HT organic thermoelectric films and power generators," *Journal of Materials Chemistry A*, vol. 3, no. 43, pp. 21428–21433, 2015 (English).

[217] M. Yu, W. Q. Tian, C. S. Jayanthi, and S. Y. Wu, "The effect of humidity on the adsorption of the hydrazine on single-wall carbon nanotubes: first-principles electronic structure calculations," *Chemical Physics Letters*, vol. 518, pp. 93–98, 2011.

[218] C. Klinke, J. Chen, A. Afzali, and P. Avouris, "Charge transfer induced polarity switching in carbon nanotube transistors," *Nano Letters*, vol. 5, no. 3, pp. 555–558, 2005.

[219] C. Yu, A. Murali, K. Choi, and Y. Ryu, "Air-stable fabric thermoelectric modules made of N- and P-type carbon nanotubes," *Energy & Environmental Science*, vol. 5, no. 11, pp. 9481–9486, 2012.

[220] D. D. Freeman, K. Choi, and C. Yu, "N-type thermoelectric performance of functionalized carbon nanotube-filled polymer composites," *PLoS ONE*, vol. 7, no. 11, p. e47822, 2012.

[221] C. Cho, M. Culebras, K. L. Wallace et al., "Stable n-type thermoelectric multilayer thin films with high power factor from carbonaceous nanofillers," *Nano Energy*, vol. 28, pp. 426–432, 2016 (English).

[222] D. Yoo, J. Kim, S. H. Lee et al., "Effects of one- and two-dimensional carbon hybridization of PEDOT:PSS on the power factor of polymer thermoelectric energy conversion devices," *Journal of Materials Chemistry A*, vol. 3, no. 12, pp. 6526–6533, 2015 (English).

[223] C. A. Hewitt, A. B. Kaiser, S. Roth, M. Craps, R. Czerw, and D. L. Carroll, "Multilayered carbon nanotube/polymer composite based thermoelectric fabrics," *Nano Letters*, vol. 12, no. 3, pp. 1307–1310, 2012.

[224] D. Olaya, M. Hurtado-Morales, D. Gómez, O. A. Castañeda-Uribe, Z. Juang, and Y. Hernández, "Large thermoelectric figure of merit in graphene layered devices at low temperature," *2D Materials*, vol. 5, no. 1, p. 011004, 2017.

[225] J. Dong, W. Liu, H. Li, X. Su, X. Tang, and C. Uher, "In situ synthesis and thermoelectric properties of PbTe-graphene nanocomposites by utilizing a facile and novel wet chemical method," *Journal of Materials Chemistry A*, vol. 1, no. 40, pp. 12503–12511, 2013.

[226] S. D. Yang, J. X. Si, Q. M. Su, and H. F. Wu, "Enhanced thermoelectric performance of SnSe doped with layered MoS2/graphene," *Materials Letters*, vol. 193, pp. 146–149, 2017 (English).

[227] F. Chu, Q. H. Zhang, Z. X. Zhou, D. K. Hou, L. J. Wang, and W. Jiang, "Enhanced thermoelectric and mechanical properties of Na-doped polycrystalline SnSe thermoelectric materials via CNTs dispersion," *Journal of Alloys and Compounds*, vol. 741, pp. 756–764, 2018.

[228] B. Khasimsaheb, N. K. Singh, S. Bathula, B. Gahtori, D. Haranath, and S. Neeleshwar, "The effect of carbon nanotubes (CNT) on thermoelectric properties of lead telluride (PbTe) nanocubes," *Current Applied Physics*, vol. 17, no. 2, pp. 306–313, 2017.

[229] Y. Son, M. L. Cohen, and S. G. Louie, "Half-metallic graphene nanoribbons," *Nature*, vol. 444, no. 7117, pp. 347–349, 2006.

[230] K. Kuroki and R. Arita, "'Pudding Mold' band drives large thermopower in NaxCoO2," *Journal of the Physical Society of Japan*, vol. 76, no. 8, p. 083707, 2007.

[231] T. Ouyang, Y. P. Chen, K. K. Yang, and J. X. Zhong, "Thermal transport of isotopic-superlattice graphene nanoribbons with zigzag edge," *EPL (Europhysics Letters)*, vol. 88, no. 2, p. 28002, 2009.

[232] X. K. Chen, Z. X. Xie, W. X. Zhou, and K. Q. Chen, "The thermal conductivity in hybridised graphene and boron nitride nanoribbons modulated with strain," *Journal of Physics D: Applied Physics*, vol. 49, no. 11, p. 115301, 2016 (English).

[233] I. M. Felix and L. F. Pereira, "Thermal conductivity of graphene-hBN superlattice ribbons," *Scientific Reports*, vol. 8, no. 1, p. 2737, 2018.

[234] J. W. Jiang, J. S. Wang, and B. S. Wang, "Minimum thermal conductance in graphene and boron nitride superlattice," *Applied Physics Letters*, vol. 99, no. 4, p. 043109, 2011 (English).

[235] X. Mu, L. L. Wang, X. M. Yang, P. Zhang, A. C. To, and T. F. Luo, "Ultra-low thermal conductivity in Si/Ge hierarchical superlattice nanowire," *Scientific Reports*, vol. 5, no. 1, 2015 (English).

[236] Y. Wang, X. L. Ruan, and A. K. Roy, "Two-temperature nonequilibrium molecular dynamics simulation of thermal transport across metal-nonmetal interfaces," *Physical Review B: Condensed Matter and Materials Physics*, vol. 85, no. 20, p. 205311, 2012.